07-04-2018
hep-ph/07-04-2018

Higgs boson production at the LHC using the q_T subtraction formalism at N^{3}LO QCD

Leandro Cieri[(a,b)], **Xuan Chen**[(b)], **Thomas Gehrmann**[(b)], **E.W.N. Glover**[(c)] and **Alexander Huss**[(d)]

[(a)] INFN, Sezione di Milano-Bicocca,
Piazza della Scienza 3, I-20126 Milano, Italy

[(b)] Physik-Institut, Universität Zürich, CH-8057 Zurich, Switzerland

[(c)] Institute for Particle Physics Phenomenology, Durham University, Durham, DH1 3LE, UK

[(d)] Theoretical Physics Department, CERN, 1211 Geneva 23, Switzerland

Abstract

We consider higher-order QCD corrections to Higgs boson production through gluon–gluon fusion in the large top quark mass limit in hadron collisions. We use the transverse-momentum (q_T) subtraction method at the next-to-next-to-next-to-leading order (N^{3}LO) joint with the NNLO Higgs plus jet framework to numerically compute completely differential infrared-safe observables for this class of processes. To cancel the infrared divergences, we exploit the universal behaviour of the associated q_T distributions in the small-q_T region. We document all the necessary ingredients of the transverse-momentum subtraction method up to N^{3}LO. The missing third order collinear functions, which contributes only at $q_T = 0$, are approximated using a prescription which requires the use of the total Higgs boson cross section at N^{3}LO. As an application of the third order q_T subtraction method, we present the N^{3}LO rapidity distribution of the Higgs boson at the LHC.

07-04-2018
April 2018

1 Introduction

The most straightforward and successful (as well as systematically improvable) strategy of calculation in QCD, at high-momentum scales Q, is to use a perturbative approximation, involving a series expansion in the strong coupling $\alpha_S(Q^2)$. Therefore the cross sections are written as a series expansion in the parameter α_S and an improvement in accuracy is obtained by calculating one further coefficient in the series. Until few years ago, the standard for such calculations was next-to-leading order (NLO) accuracy. But after the next-to-next-to-leading order (NNLO) *revolution* which started in the first decade of the twenty-first century, the standard precision for LHC phenomenology became the second non trivial order in the strong coupling α_S for many of the most important processes of interest.

Among the motivations of the extension from NLO to NNLO accuracy, reduce the theoretical uncertainties was one of the main objectives. In particular, this extension is certainly important in two cases. One of them is related with those processes whose NLO corrections are comparable to the leading order (LO) contribution. Alternatively, in those ‘‘benchmark’’ processes that are measured with high experimental precision and the extraction of precise information about Standard-Model (SM) couplings (as for the Higgs boson) or parton-distribution functions from measured cross-sections would be limited by the accuracy of the theoretical calculation rather than the measurement. Such improvement in the accuracy of the calculation however, implies finding methods and techniques to practically achieve the cancellation of infrared (IR) divergences that appear at intermediate steps of the calculations. The past recent years were witness of a great development in NNLO subtractions prescriptions. The transverse momentum (q_T) subtraction method [1, 2, 3], the N-jettiness subtraction [4, 5] and the Antenna method [7] belong to the most used NNLO subtraction prescriptions.

Besides the success of the NNLO subtraction program, the large centre–of–mass energies reached at the LHC and the continuously increasing accuracy of the performed measurements, the NNLO reveals itself (in some cases) even not enough to describe properly the LHC data. In many processes in which the size of the NLO corrections were comparable with the LO, the NNLO corrections presented large corrections and the size of theoretical uncertainties was not satisfactory at the light of the new LHC precision. The precedent reasons originated in the past few months the beginning of a new extension program from the NNLO to the next subsequent perturbative order: the next-to-next-to-next-to-leading order (N^{3}LO).

Among several estibalished N^{3}LO calculations, Higgs rapidity distribution has been studied through exapnsion of the analytical N^{3}LO coefficient functions around the production threshold of the Higgs boson [6]. Contribution from the first two orders of threshold expansion has been calculated for Higgs rapidity distribution and detailed numerical impact of joining these contributions with full NNLO resutls has been illustrated.

In this paper we present for first time the extension of the q_T subtraction program at N^{3}LO and its application to the Higgs boson production. The paper is organized as follows: in Sec. 2 we recall briefly the main ideas of the q_T subtraction formalism and we present its necessary ingredients up to N^{3}LO, specifying which elements are known analytically and the missing coefficients at N^{3}LO. In Sec. 3 we present a prescription in order to approximate the missing collinear functions at N^{3}LO based on the unitarity property of the total integral of the transverse momentum distribution. In

Sec. 4 we apply the q_T subtraction formalism at N^{3}LO in order to produce completely differential distributions in the particular case of the rapidity of the Higgs boson. In Sec. 4.1 we quantify the quality of the approximation made in Sec. 3 performing an exercise at NNLO where all the q_T subtraction ingredients are known. Our first N^{3}LO results concerning the rapidity of the Higgs boson are presented in Sec. 4.2, where we estimate the uncertainties introduced by the use of the technical cut $q_T^{\rm cut}$ and the approximation introduced in Sec. 3 at N^{3}LO. In Sec. 4.3 we present the final results regarding our best estimation of the Higgs boson rapidity at N^{3}LO and its comparison with the rapidities of the previous orders. Finally, in Sect. 5 we summarize our results.

2 The q_T subtraction formalism at N^{3}LO

This section is devoted to the presentation of the transverse-momentum subtraction formalism at N^{3}LO in perturbative QCD. The method is illustrated in general form and special attention is paid to the case of Higgs boson production through gluon–gluon fusion. The q_T subtraction formalism presented in this section is the third order extension of the subtraction method originally proposed in Refs. [1, 2, 3].

We consider the inclusive hard-scattering reaction

$$h_1(p_1) + h_2(p_2) \to F(\{q_i\}) + X \,, \tag{1}$$

where h_1 and h_2 are the two hadrons which collide with momenta p_1 and p_2 producing the triggered final-state system F, accompanied by an arbitrary and undetected final state X. The colliding hadrons with centre–of–mass energy $\sqrt{s}$, are treated as massless particles ($s = (p_1+p_2)^2 = 2p_1p_2$). The observed final state F consist of a generic system of non-QCD partons composed by *one* or *more* colour singlet particles (such as *one* or *more* vector bosons $(\gamma^*, W, Z, \dots)$, photons, Higgs particles, Drell–Yan (DY) lepton pairs and so forth) with momenta q_i^μ $(i = 3, 4, 5, \dots)$. The total momentum of the system F is denoted by q^μ $(q = \sum_i q_i)$ and it can be expressed in terms of the total invariant mass M $(q^2 = M^2)$, the transverse momentum $\mathbf{q_T}$ with respect to the direction of the colliding hadrons, and the rapidity y $(2y = \ln(p_2q/p_1q))$ in the centre–of–mass system of the collision. Since F is colourless, the LO partonic Born cross section can be either initiated by qq' annihilation , as in the case of the Drell–Yan process or by gluon–gluon fusion as in the case of the Higgs boson production.

In order to report the structure of the subtraction formalism we first notice that at LO, the transverse momentum $\boldsymbol{q}_T = \sum_i \boldsymbol{q}_{T\,i}$ of the final state system F is identically zero. Therefore, as long as $q_T \neq 0$, the N^{n}LO QCD contributions (with $n = 1, 2, 3$) are given by the N^{n-1}LO QCD contributions to the triggered final state F+jet(s). Consequently, if $q_T \neq 0$ we have:

$$d\sigma^F_{\rm N^nLO}(q_T \neq 0) \equiv d\sigma^{F+\rm jets}_{\rm N^{n-1}LO} \quad \text{with} \quad n = 1, 2, 3 \,. \tag{2}$$

The notation N^{n}LO stands for: N^{0}LO=LO, N^{1}LO=NLO, N^{2}LO=NNLO and so forth. Equation (2) implies that if $q_T \neq 0$ the infra–red (IR) divergencies that appear in the computation of $d\sigma^F_{\rm N^nLO}(q_T \neq 0)$ are those already present in $d\sigma^{F+\rm jets}_{\rm N^{n-1}LO}$. The IR singularities involved in $d\sigma^F_{\rm N^nLO}(q_T \neq 0)$ can be handled and cancelled with the available subtraction methods at N^{n-1}LO. The only remaining singularities at N^{n}LO are associated with the limit $q_T \to 0$ and we treat them with the transverse momentum subtraction method. Since the small-q_T behaviour of the transverse momentum cross section is well known thorough the resummation program [8] of logarithmically-enhanced contributions to transverse-momentum distributions, we exploit this knowledge to construct the necessary counterterms (CT) in order to subtract the remaining singularity promoting the q_T subtraction method proposed in Refs. [1, 2, 3] to N^{3}LO.

The sketchy form of the q_T subtraction method [1] for the N^{n}LO cross section is

$$d\sigma^{F}_{\mathrm{N^nLO}} = \mathcal{H}^{F}_{\mathrm{N^nLO}} \otimes d\sigma^{F}_{\mathrm{LO}} + \left[d\sigma^{F+\mathrm{jets}}_{\mathrm{N^{n-1}LO}} - d\sigma^{F\,\mathrm{CT}}_{\mathrm{N^nLO}} \right] \quad \text{with} \quad n = 1, 2, 3 \; , \tag{3}$$

where $d\sigma^{F\,\mathrm{CT}}_{\mathrm{N^nLO}}$ is the contribution of the counterterm to the N^{n}LO cross section which cancels the divergencies of $d\sigma^{F+\mathrm{jets}}_{\mathrm{N^{n-1}LO}}$ in the limit $q_T \to 0$. The n-order counterterm can be written

$$d\sigma^{F\,\mathrm{CT}}_{\mathrm{N^nLO}} = \Sigma^{F}_{\mathrm{N^nLO}}(q_T^2/M^2)\; d^2\boldsymbol{q}_T \otimes d\sigma^{F}_{\mathrm{LO}} \; , \tag{4}$$

where the symbol $\otimes$ manifests convolutions over momentum fractions and sum over flavour indices of the partons. More precisely, the function $\Sigma^{F}_{\mathrm{N^nLO}}(q_T^2/M^2)$ is the n-order truncation of the perturbative series in α_{S}

$$\Sigma^{F}_{c\bar{c}\leftarrow a_1 a_2}(q_T^2/M^2) = \sum_{n=1}^{\infty} \left(\frac{\alpha_{\mathrm{S}}}{\pi}\right)^n \Sigma^{F;(n)}_{c\bar{c}\leftarrow a_1 a_2}(q_T^2/M^2) \; , \tag{5}$$

where the labels a_1 and a_2 stands for the partonic channels of the N^{n}LO correction to the Born cross section ($d\sigma^{F}_{\mathrm{LO}} \equiv d\big[\sigma^{F;(0)}_{c\bar{c}}\big]$). Notice that at LO the only available configuration is $a_1 = c$ and $a_2 = \bar{c}$, where $c\bar{c}$ is (are) the partonic channel(s) at which the LO cross section is initiated. The function $\Sigma^F(q_T^2/M^2)$ embodies all the logarithmic terms that are divergent in the limit $q_T \to 0$ reproducing the singular behaviour of $d\sigma^{F+\mathrm{jets}}$ in the small-q_T limit. The counterterm is defined free of terms proportional to $\delta(q_T^2)$ which are all considered in the perturbative factor $\mathcal{H}^F$. The hard coefficient function $\mathcal{H}^{F}_{\mathrm{N^nLO}}$ that encodes all the IR finite terms of the n-loop contributions, is obtained by the N^{n}LO truncation of the perturbative function

$$\mathcal{H}^{F}_{c\bar{c}\leftarrow a_1 a_2}(z;\alpha_{\mathrm{S}}) = \delta_{c\,a_1}\,\delta_{\bar{c}\,a_2}\;\delta(1-z) + \sum_{n=1}^{\infty}\left(\frac{\alpha_{\mathrm{S}}}{\pi}\right)^n \mathcal{H}^{F;(n)}_{c\bar{c}\leftarrow a_1 a_2}(z) \;\; , \tag{6}$$

where $z = M^2/s$. According to the transverse momentum resummation formula (Eq. (10) of Ref. [2]) and using the Fourier transformation between the conjugate variables q_T and b (b is the impact parameter), the perturbative hard function $\mathcal{H}^F$ and the counterterm are obtained by the fixed order truncation of the following identity

$$\begin{aligned}\Big(\Sigma^{F}_{c\bar{c}\leftarrow a_1 a_2}(q_T^2/M^2) + \mathcal{H}^{F}_{c\bar{c}\leftarrow a_1 a_2}(M^2/s;\alpha_{\mathrm{S}})\Big) \otimes d\big[\hat{\sigma}^{F;(0)}_{c\bar{c}}\big] &= \frac{M^2}{s}\int_0^\infty db\,\frac{b}{2} J_0(bq_T)\; S_c(M,b) \\ \times \int_{x_1}^{1}\frac{dz_1}{z_1}\int_{x_2}^{1}\frac{dz_2}{z_2} d\hat{\sigma}^{F;(0)}_{c\bar{c}}\; f_{a_1/h_1}\left(x_1/z_1, b_0^2/b^2\right) f_{a_2/h_2}\left(x_2/z_2, b_0^2/b^2\right) &\otimes \big[H^F C_1 C_2\big]_{c\bar{c};a_1 a_2} \; ,\end{aligned} \tag{7}$$

where $J_0(bq_T)$ is the 0th-order Bessel function, $f_{c/h}$ corresponds to the distribution of a parton c in a hadron h and $b_0 = 2e^{-\gamma_E}$ ($\gamma_E = 0.5772...$ is the Euler number). The symbolic factor $d\hat{\sigma}^{F;(0)}_{c\bar{c}}$ for the partonic Born cross section $\hat{\sigma}^{F;(0)}_{c\bar{c}}$ denotes

$$d\hat{\sigma}^{F;(0)}_{c\bar{c}} \equiv \frac{d\hat{\sigma}^{F;(0)}_{c\bar{c}}}{d\phi} \; , \tag{8}$$

where ϕ represents the phase–space of the final state system F. In the left hand side of Eq. (7) the convolution (as well as sum over flavour indices of the partons) between the resummation functions $\Sigma^F_{c\bar{c}}$ and $\mathcal{H}^F_{c\bar{c}}$, the partonic Born cross section and the parton distributions is symbolically denoted by $\otimes d\big[\hat{\sigma}^{F;(0)}_{c\bar{c}}\big]$.

The large logarithmic corrections are exponentiated in the Sudakov form factor $S_c(M,b)$ of the quark ($c = q, \bar{q}$) or of the gluon ($c = g$), and it has the following expression:

$$S_c(M,b) = \exp\left\{ -\int_{b_0^2/b^2}^{M^2} \frac{dq^2}{q^2} \left[A_c(\alpha_S(q^2)) \, \ln\frac{M^2}{q^2} + B_c(\alpha_S(q^2)) \right] \right\} \quad . \tag{9}$$

The functions A and B in Eq. (9) are perturbative series in α_S:

$$A_c(\alpha_S) = \sum_{n=1}^{\infty} \left(\frac{\alpha_S}{\pi}\right)^n A_c^{(n)} \quad , \tag{10}$$

$$B_c(\alpha_S) = \sum_{n=1}^{\infty} \left(\frac{\alpha_S}{\pi}\right)^n B_c^{(n)} \quad . \tag{11}$$

The structure of the symbolic factor denoted by $\big[H^{F=H} C_1 C_2\big]_{c\bar{c};a_1a_2}$ which depends strongly on the initial state channel of the Born subprocess, is explained with detail in Refs. [10, 11]. Here we limit ourselves to the case in which the final state system F is composed by a single Higgs boson

$$\begin{aligned} \big[H^{F=H} C_1 C_2\big]_{gg;a_1a_2} &= H_g^{F=H}(\alpha_S(M^2)) \; \big[\, C_{g\,a_1}(z_1;\alpha_S(b_0^2/b^2)) \; C_{g\,a_2}(z_2;\alpha_S(b_0^2/b^2)) \\ &+ G_{g\,a_1}(z_1;\alpha_S(b_0^2/b^2)) \; G_{g\,a_2}(z_2;\alpha_S(b_0^2/b^2)) \,\big] \quad . \end{aligned} \tag{12}$$

The right-hand side of Eq. (12) does not depend on the direction of $\mathbf{b}$ and this implies that the $\mathbf{q_T}$ distribution has no azimuthal correlations in the small-q_T region for Higgs boson production [10]. The presence of the $G_{g\,a}(z;\alpha_S)$ functions in the right–hand side of Eq. (12) is the manifestation of the helicity-flip contributions. Since in Eq. (12) there are contributions with two $G_{g\,a}(z;\alpha_S)$ functions, for Higgs boson production there are only double helicity-flip terms; helicity conservation in the hard-process factor for Higgs boson production forbids contributions that are produced by a single helicity-flip. The helicity-flip $G_{g\,a}(z;\alpha_S)$ functions are absent in processes initiated at the Born level by quark annihilation [10]. The gluonic hard–collinear coefficient function $C_{g\,a}(z;\alpha_S)$ ($a = q, \bar{q}, g$) in the right-hand side of Eq. (12) has the following perturbative structure

$$C_{g\,a}(z;\alpha_S) = \delta_{g\,a} \;\; \delta(1-z) + \sum_{n=1}^{\infty} \left(\frac{\alpha_S}{\pi}\right)^n C_{g\,a}^{(n)}(z) \quad . \tag{13}$$

At variance with Eq. (13), the perturbative expansion of the coefficient functions G_{ga}, which are specific to gluon-initiated processes, starts at $\mathcal{O}(\alpha_S)$, and we write [10, 11]

$$G_{g\,a}(z;\alpha_S) = \frac{\alpha_S}{\pi} \; G_{g\,a}^{(1)}(z) \; + \sum_{n=2}^{\infty} \left(\frac{\alpha_S}{\pi}\right)^n G_{g\,a}^{(n)}(z) \quad . \tag{14}$$

The IR finite contribution of the n-loop correction terms to the Born subprocess are embodied in the hard-virtual function

$$H_g^{F=H}(\alpha_S) = 1 + \sum_{n=1}^{\infty} \left(\frac{\alpha_S}{\pi}\right)^n H_g^{F=H\,;(n)} \quad . \tag{15}$$

We now turn to the discussion of the resummation scheme dependence of the coefficient functions. The resummation formula (7) is invariant under the following 'resummation scheme' transformations [12]:

$$\begin{aligned}
H_c^F(\alpha_S) &\to H_c^F(\alpha_S)\ [h(\alpha_S)]^{-1} \ , \\
B_c(\alpha_S) &\to B_c(\alpha_S) - \beta(\alpha_S)\ \frac{d\ln h(\alpha_S)}{d\ln\alpha_S} \ , \\
C_{ab}(\alpha_S, z) &\to C_{ab}(\alpha_S, z)\ [h(\alpha_S)]^{1/2} \ , \\
G_{ab}(\alpha_S, z) &\to G_{ab}(\alpha_S, z)\ [h(\alpha_S)]^{1/2} \ .
\end{aligned} \tag{16}$$

The invariance can easily be proven by using the following renormalization-group identity:

$$h(\alpha_S(b_0^2/b^2)) = h(\alpha_S(M^2))\ \exp\left\{ - \int_{b_0^2/b^2}^{M^2} \frac{dq^2}{q^2}\ \beta(\alpha_S(q^2))\ \frac{d\ln h(\alpha_S(q^2))}{d\ln\alpha_S(q^2)} \right\} \ , \tag{17}$$

which is valid for any perturbative function $h(\alpha_S)$. Notice that Eq. (17) establishes the evolution of the perturbative functions from the scale $q^2 = b_0^2/b^2$ to $q^2 = M^2$. The QCD β function and its corresponding n-order β_n coefficient are defined as

$$\frac{d\ln\alpha_S(\mu^2)}{d\ln\mu^2} = \beta(\alpha_S(\mu^2)) = -\sum_{n=0}^{+\infty} \beta_n \left(\frac{\alpha_S}{\pi}\right)^{n+1} \ . \tag{18}$$

The explicit expression of the first three coefficients [13, 14], β_0, β_1 and β_2 are

$$\begin{aligned}
\beta_0 &= \frac{1}{12}\left(11C_A - 2N_f\right) \ , \qquad \beta_1 = \frac{1}{24}\left(17C_A^2 - 5C_AN_f - 3C_FN_f\right) \ , \\
\beta_2 &= \frac{1}{64}\left(\frac{2857}{54}C_A^3 - \frac{1415}{54}C_A^2N_f - \frac{205}{18}C_AC_FN_f + C_F^2N_f + \frac{79}{54}C_AN_f^2 + \frac{11}{9}C_FN_f^2\right) \ ,
\end{aligned} \tag{19}$$

where N_f is the number of QCD massless flavours and the $SU(N_c)$ colour factors are $C_A = N_c$ and $C_F = (N_c^2-1)/(2N_c)$.

The physical origin of the resummation scheme invariance of Eq. (7) is discussed in Ref. [12]. The invariance implies that the hard-virtual factors H_c^F, S_c (more precisely, the function B_c) and C_{ab} are not unambiguously computable order by order in perturbation theory. After choosing a 'resummation scheme', these factors can be unambiguously defined. We rely on the *hard resummation scheme* defined in Ref. [11], which states all the contributions proportional to $\delta(1-z)$ are considered in the hard-virtual functions H_c^F. The precedent condition directly implies that H_c^F is process dependent whereas the collinear C_{ab} functions and the resummation coefficients B_c are independent of the final state system F. In addition, the resummation coefficients A_c and the helicity-flip functions G_{ab} are also independent of the final state process.

The truncation of Eq. (7) at a given fixed order requieres the explicit use of several resummation coefficients and hard collinear coefficient functions. At NLO, the coefficients $A_g^{(1)}$, $B_g^{(1)}$, $C_{ga}^{(1)}$ ($a = q, \bar{q}, g$) and $H_g^{H;(1)}$ are enough to compute the inclusive total cross section and differential distributions. Assuming that the Higgs boson couples to a single heavy quark of mass m_Q, the first-order coefficient $H_g^{H;(1)}$ in the hard scheme is [11]

$$H_g^{H;(1)} = C_A\pi^2/2 + c_H(m_Q) \, . \tag{20}$$

The function $c_H(m_Q)$, which depends on the NLO virtual corrections of the Born subprocess $d\sigma^F_{\rm LO}$, is given in Eq. (B.2) of Ref. [27]. In the limit $m_Q \to \infty$, the function c_H becomes

$$c_H(m_Q) \longrightarrow \frac{5C_A - 3C_F}{2} = \frac{11}{2} \,. \tag{21}$$

Therefore the complete NLO set of necessary coefficients to compute Higgs boson production, in the limit in which the mass of the heavy quark Q (the top quark $Q = t$) is larger than any other scale involved in the process ($M_H \ll m_t$) is

$$\begin{aligned} A_g^{(1)} &= C_A \,, \qquad B_g^{(1)} = -\frac{1}{6}\left(11 C_A - 2 N_f\right) \,, \qquad H_g^{H;(1)} = \frac{1}{2}(11 + C_A \pi^2) \,, \\ C_{ga}^{(1)}(z) &= \frac{1}{2} C_F\, z \qquad [a = q, \bar{q}] \,, \qquad C_{gg}^{(1)}(z) = 0 \,. \end{aligned} \tag{22}$$

The coefficients $A_g^{(1)}$ and $B_g^{(1)}$ are process as well as resummation scheme independent. In the hard resummation scheme the collinear functions $C_{ga}^{(1)}$ ($a = q, \bar{q}, g$) are process independent whereas $H_g^{H;(1)}$ depends on final state system ($F = H$), and both depend on the resummation scheme in such a way to ensure the resummation scheme independence of Eq. (7) at NLO. The computation of the hard-virtual coefficients $H_c^{H;(1)}$ requires the definition of a specific prescription [24]. The explicit calculations and the results of Ref. [24] show that the NLO hard-virtual coefficient $H_c^{F;(1)}$ is explicitly related in a process-independent form to $d\hat{\sigma}^F_{\rm LO}$ and to the IR finite part of the NLO virtual correction to the Born cross section. The precedent process-independent relation is based on the definition of universal subtraction operators that cancel the IR divergences of the one-loop (NLO) virtual correction to the Born cross section and fix the first order IR finite constant δ_{q_T} [11]. The coefficient δ_{q_T}, that only depends on the initial state partons, has a *soft* origin and it is defined in Refs. [24] and [11].

At NNLO, the coefficients $A_g^{(2)}$ and $B_g^{(2)}$ are needed [2, 11],

$$A_g^{(2)} = \frac{1}{2}\, C_A \left[\left(\frac{67}{18} - \frac{\pi^2}{6} \right) C_A - \frac{5}{9} N_f \right] \,, \qquad B_g^{(2)} = \frac{\gamma_{g(1)}}{16} + \beta_0\, C_A\, \zeta_2 \,, \tag{23}$$

where $\gamma_{g(1)}$ is the coefficient of the $\delta(1-z)$ term in the NLO gluon splitting functions [18, 19], which reads

$$\gamma_{g\,(1)} = \left(-\frac{64}{3} - 24\zeta_3 \right) C_A^2 + \frac{16}{3}\, C_A N_f + 4\, C_F N_f \,, \tag{24}$$

and ζ_n is the Riemann zeta-function ($\zeta_2 = \pi^2/6, \zeta_3 = 1.202\ldots, \zeta_4 = \pi^4/90$). The coefficient $A_g^{(2)}$ does not depend on the resummation scheme whereas $B_g^{(2)}$ in Eq. (23) is expressed in the hard resummation scheme and both coefficients are process independent. The collinear functions $C_{ga}^{(2)}$ ($a = q, \bar{q}, g$) in the hard resummation scheme can be extracted from Refs. [11, 16] and they are independent of the final state system F.

The general structure of the hard-virtual coefficients H_c^F has been established only recently [11]. Although this factor is process dependent, in Ref. [11] was shown that it can be directly related in a universal (process-independent) way to the IR finite part of the all-order virtual amplitude of the corresponding partonic subprocess $c\bar{c} \to F$. The precedent relation between H_c^F and the all-order virtual correction to the partonic subprocess $c\bar{c} \to F$ is explicitly known up to the NNLO and it is based on the definition of universal subtraction operators that cancel the IR divergences of the two-loop (NNLO) virtual corrections to the Born cross section. These universal second order operators contain an IR finite term of soft origin ($\delta_{q_T}^{(1)}$) that only depends on the initial state partons [11].

In the case of Higgs boson production the hard-virtual factor $H_g^{F=H;(2)}$ in the large-m_t limit (in the hard scheme) is [16]

$$\begin{aligned} H_g^{H;(2)} = & C_A^2 \left(\frac{3187}{288} + \frac{7}{8} L_t + \frac{157}{72} \pi^2 + \frac{13}{144} \pi^4 - \frac{55}{18} \zeta_3 \right) + C_A C_F \left(-\frac{145}{24} - \frac{11}{8} L_t - \frac{3}{4} \pi^2 \right) \\ & + \frac{9}{4} C_F^2 - \frac{5}{96} C_A - \frac{1}{12} C_F - C_A N_f \left(\frac{287}{144} + \frac{5}{36} \pi^2 + \frac{4}{9} \zeta_3 \right) + C_F N_f \left(-\frac{41}{24} + \frac{1}{2} L_t + \zeta_3 \right) , \end{aligned} \tag{25}$$

where $L_t = \ln(M^2/m_t^2)$. The two-loop scattering amplitude [20] used in the computation of $H_g^{F=H;(2)}$ includes corrections to the large-m_t approximation (the evaluation of the corrections uses the expansion parameter $1/m_t^2$). At NNLO, in Eq. (12) (which is proportional to $\delta(q_T^2)$) the first order $G_{ga}^{(1)}$ helicity-flip functions are also needed and they read [10]

$$G_{g\,a}^{(1)}(z) = C_a \, \frac{1-z}{z} \qquad\qquad a = q, \bar{q}, g \, . \tag{26}$$

The first-order functions $G_{ga}^{(1)}$ are resummation-scheme independent and they do not depend on the final state system F.

At N^{3}LO, the numerical implementation of Eq. (7) requieres the following ingredients: $A_g^{(3)}$, $B_g^{(3)}$, $C_{ga}^{(3)}$, $G_{ga}^{(2)}$ $(a = q, \bar{q}, g)$ and $H_g^{H;(3)}$. The coefficient $A_g^{(3)}$ [31] reads

$$\begin{aligned} A_g^{(3)} & = C_A^3 \left(\frac{245}{96} - \frac{67}{36} \zeta_2 + \frac{11}{24} \zeta_3 + \frac{11}{20} \zeta_2^2 \right) + C_A C_F N_f \left(-\frac{55}{96} + \frac{1}{2} \zeta_3 \right) - C_A N_f^2 \frac{1}{108} \\ & + \; C_A^2 N_f \left(-\frac{209}{432} + \frac{5}{18} \zeta_2 - \frac{7}{12} \zeta_3 \right) + \beta_0 C_A^2 \left(\frac{101}{27} - \frac{7}{2} \zeta_3 \right) - \beta_0 C_A N_f \frac{14}{27} \, . \end{aligned} \tag{27}$$

The explicit expression of the $B_c^{(3)}$ $(a = q, g)$ coefficients in the hard scheme can be computed from Refs. [28, 29]. In the particular case of the gluon channel we have

$$\begin{aligned} B_g^{(3)} \;\; = & \;\; -\frac{2133}{64} + \frac{3029}{576} N_f - \frac{349}{1728} N_f^2 + \frac{109}{6} \pi^2 - \frac{283}{144} \pi^2 N_f + \frac{5}{108} \pi^2 N_f^2 - \frac{253}{160} \pi^4 + \frac{23}{240} \pi^4 N_f \\ - & \;\; \frac{843}{8} \zeta_3 + 2 \zeta_3 N_f + \frac{1}{6} \zeta_3 N_f^2 + \frac{9}{4} \pi^2 \zeta_3 + \frac{135}{2} \zeta_5 \, . \end{aligned} \tag{28}$$

The analytical form of the function $\Sigma^{F;(3)}$ in Eq. (7) can be obtained by expanding the Sudakov form factor to the matching order in hard resummation scheme. The full analytical formulae for Σ^F are resummation scheme dependent. However, the logarithmic singular behaviours for Σ^F at $q_T \to 0$ should be the same and can be validated through comparisons with fixed order results at small q_T. More specifically, the LO Higgs q_T distribution was validated with singular contribution from NLL (next-to-leading-logarithm) resummation [21, 22], the NLO Higgs q_T distribution was validated with singular contribution from NNLL resummation [23, 24], the NNLO Higgs q_T distribution has been recently validated with singular contribution from N^{3}LL resummation [25, 26]. A separate study joining q_T subtraction formalism with resummation is expected in the future as an extansion of the current N^{3}LO calculation.

The function $\mathcal{H}^{F;(3)}_{c\bar{c}\leftarrow a_1 a_2}$ which is proportional to $\delta(q_T^2)$, contains the functions $H_c^{H;(3)}$, $C_{ga}^{(3)}$ and $G_{ga}^{(2)}$ that are not completely known. Nevertheless, within our subtraction formalism, $\mathcal{H}^{F\,;(3)}$ can be determined for any hard-scattering process whose corresponding total cross section is known at N^{3}LO. This point is discussed in detail in Sect. 3.

3 The Higgs boson total cross section at N^{3}LO

We start this section with some observations related to the hard-scattering function $\mathcal{H}^F_{c\bar{c}\leftarrow ab}$. This function is resummation-scheme independent, but it depends on the specific hard-scattering sub-process $c+\bar{c}\to F$. The coefficients $\mathcal{H}^{F\,;(n)}_{c\bar{c}\leftarrow ab}$ of the perturbative expansion in Eq. (6) can be determined by performing a customary perturbative calculation of the q_T distribution in the limit $q_T\to 0$. In right-hand side of Eq. (7), within our subtraction method, the function $\mathcal{H}^F$ controls the strict perturbative normalization of the corresponding total cross section (i.e. the integral of the total q_T distribution). This unitary-related property can be exploited to determine the coefficients $\mathcal{H}^{F\,;(n)}_{c\bar{c}\leftarrow ab}$ from the perturbative calculation of the total cross section. At the partonic level, the integral of the total q_T distribution in Eq. (3) results in the total cross section $\hat{\sigma}^{\rm tot}_{F\,ab}$,

$$\hat{\sigma}^{\rm tot}_{F\,ab}(M,\hat{s};\alpha_{\rm S}(\mu_R^2),\mu_R^2,\mu_F^2)=\int_0^\infty dq_T^2\,\frac{d\hat{\sigma}_{F\,ab}}{dq_T^2}(q_T,M,\hat{s};\alpha_{\rm S}(\mu_R^2),\mu_R^2,\mu_F^2)\;. \tag{29}$$

Since the the hard-scattering function $\mathcal{H}^F_{c\bar{c}\leftarrow ab}$ is simply proportional to $\delta(q_T^2)$, we evaluate the q_T spectrum on right-hand side of Eq. (3) according to the following decomposition

$$\hat{\sigma}^{\rm tot}_{F\,ab}=\frac{M^2}{\hat{s}}\,\mathcal{H}^F_{ab}+\int_0^\infty dq_T^2\,\frac{d\hat{\sigma}^{(\rm fin.)}_{F\,ab}}{dq_T^2}\quad, \tag{30}$$

where $d\hat{\sigma}^{(\rm fin.)}_{F\,ab}$ is directly related to the quantity in square bracket in the right-hand side of Eq. (3)

$$\frac{d\hat{\sigma}^{(\rm fin.)}_{F\,ab}}{dq_T^2}\equiv\left[\frac{d\hat{\sigma}^{F+{\rm jets}}_{ab}}{dq_T^2}-\frac{d\hat{\sigma}^{F\,{\rm CT}}_{ab}}{dq_T^2}\right]\;. \tag{31}$$

Using Eqs. (7) and (12) it is possible to write $\mathcal{H}^H_{gg}$ in function of the functions $C_{g\,a}(z_1;\alpha_{\rm S})$ and $G_{g\,a}(z_1;\alpha_{\rm S})$ (in the particular case $F=H$)

$$\mathcal{H}^H_{gg\leftarrow ab}(z;\alpha_{\rm S})\equiv H_g^H(\alpha_{\rm S})\int_0^1 dz_1\int_0^1 dz_2\,\delta(z-z_1z_2)\Big[C_{g\,a}(z_1;\alpha_{\rm S})C_{g\,b}(z_2;\alpha_{\rm S})+G_{g\,a}(z_1;\alpha_{\rm S})G_{g\,b}(z_2;\alpha_{\rm S})\Big]\,. \tag{32}$$

The precedent expression for $\mathcal{H}^F_{ab}$ was written requiring specifically $F=H$, since its form depends strongly on the initial state of the Born sub-process (i.e quark annihilation or gluon fusion). There are only two differences between Eqs. (12) and (32). The first difference is due to the fact that the function $\mathcal{H}^H$ depends on the energy fraction z, since the right-hand side of Eq. (32) involves a convolution integral over the momentum fractions z_1 and z_2. The second difference regards the scale of $\alpha_{\rm S}$: in the functions $H_g^H(\alpha_{\rm S}), C(\alpha_{\rm S})$ and $G(\alpha_{\rm S})$ on the right-hand side of Eq. (32), the argument of α_S is set to the same value (this common scale is not explicitly denoted in Eq. (32)). Owing to this feature, the process-dependent function $\mathcal{H}^{H}_{gg\leftarrow ab}$ is unambiguously defined (i.e., it is independent of the specification of the resummation scheme) [12]. The $\mathcal{H}^{H}$ function in Eq. (32) can be expanded perturbatively without approximation at any order in the strong coupling constant α_S. The perturbative expansion of the function $\mathcal{H}^{H}$ directly follows from Eqs. (13)–(15) and for the first-order and second-order contributions we have

$$\mathcal{H}^{H;(1)}_{gg\leftarrow ab}(z) = \delta_{g\,a}\,\delta_{g\,b}\,\delta(1-z)\,H^{H;(1)}_{g} + \delta_{g\,a}\,C^{(1)}_{g\,b}(z) + \delta_{g\,b}\,C^{(1)}_{g\,a}(z) \quad , \tag{33}$$

$$\begin{aligned}\mathcal{H}^{H;(2)}_{gg\leftarrow ab}(z) &= \delta_{g\,a}\,\delta_{g\,b}\,\delta(1-z)\,H^{H;(2)}_{g} + \delta_{g\,a}\,C^{(2)}_{g\,b}(z) + \delta_{g\,b}\,C^{(2)}_{g\,a}(z) + H^{H;(1)}_{g}\left(\delta_{g\,a}\,C^{(1)}_{g\,b}(z) + \delta_{g\,b}\,C^{(1)}_{g\,a}(z)\right)\\ &+ \left(C^{(1)}_{g\,a}\otimes C^{(1)}_{g\,b}\right)(z) + \left(G^{(1)}_{g\,a}\otimes G^{(1)}_{g\,b}\right)(z) \ .\end{aligned} \tag{34}$$

In Eq. (34) and in the following, the symbol $\otimes$ denotes the convolution integral (i.e., we define $(g\otimes h)(z) \equiv \int_0^1 dz_1 \int_0^1 dz_2\, \delta(z - z_1 z_2)\, g(z_1)\, h(z_2)$). The new third-order contribution is

$$\begin{aligned}\mathcal{H}^{H;(3)}_{gg\leftarrow ab}(z) &= \delta_{g\,a}\,\delta_{g\,b}\,\delta(1-z)\,H^{H;(3)}_{g} + \delta_{g\,a}\,C^{(3)}_{g\,b}(z) + \delta_{g\,b}\,C^{(3)}_{g\,a}(z) + H^{H;(1)}_{g}\left(\delta_{g\,a}\,C^{(2)}_{g\,b}(z) + \delta_{g\,b}\,C^{(2)}_{g\,a}(z)\right)\\ &+ H^{H;(2)}_{g}\left(\delta_{g\,a}\,C^{(1)}_{g\,b}(z) + \delta_{g\,b}\,C^{(1)}_{g\,a}(z)\right) + \left(C^{(1)}_{g\,a}\otimes C^{(2)}_{g\,b}\right)(z) + \left(C^{(2)}_{g\,a}\otimes C^{(1)}_{g\,b}\right)(z)\\ &+ \left(G^{(1)}_{g\,a}\otimes G^{(2)}_{g\,b}\right)(z) + \left(G^{(2)}_{g\,a}\otimes G^{(1)}_{g\,b}\right)(z) + H^{H;(1)}_{g}\left(C^{(1)}_{g\,a}\otimes C^{(1)}_{g\,b}\right)(z)\\ &+ H^{H;(1)}_{g}\left(G^{(1)}_{g\,a}\otimes G^{(1)}_{g\,b}\right)(z) \ .\end{aligned} \tag{35}$$

The perturbative functions $C^{(1)}_{g\,a}(z)$, $C^{(2)}_{g\,a}(z)$, $G^{(1)}_{g\,a}(z)$, $H^{H;(1)}_{g}$ and $H^{H;(2)}_{g}$ are reported in Sec. 2, and therefore the coefficient functions $\mathcal{H}^{H;(1)}$ and $\mathcal{H}^{H;(2)}$ are known analytically. As stated in Sec. 2, the second-order helicity-flip functions $G^{(2)}_{g\,a}(z)$ and the third-order collinear functions $C^{(3)}_{g\,a}(z)$ are not analytically known implying that the third order $\mathcal{H}^{H;(3)}$ function can only be obtained numerically. In addition, the third-order hard-virtual coefficient $H^{H;(3)}_{g}$ is not fully analytical determined.

The relation in Eq. (30) is valid order by order in QCD perturbation theory. Once the perturbative coefficients of the fixed-order expansions of $\hat{\sigma}^{\rm tot}_{F\,ab}$, $\mathcal{H}^{F}_{ab}$ and $d\hat{\sigma}^{(\rm fin.)}_{F\,ab}/dq_T^2$ are all known, the relation (30) has to be regarded as an identity, which can be explicitly checked. Since the fixed-order truncation of $d\hat{\sigma}^{(\rm fin.)}_{F\,ab}/dq_T^2$ does not contain any contributions proportional to $\delta(q_T^2)$, $\left[d\hat{\sigma}^{(\rm fin.)}_{F\,ab}/dq_T^2\right]_{\rm NLO}$ does not explicitly depend on the coefficient $\mathcal{H}^{F\,;(1)}_{ab}$. Analogously, $\left[d\hat{\sigma}^{(\rm fin.)}_{F\,ab}/dq_T^2\right]_{\rm NNLO}$ does not explicitly depend on the coefficient $\mathcal{H}^{F\,;(2)}_{ab}$, and so forth. Therefore, Eq. (30) can be used to determine the N$^{\rm n}$LO coefficient $\mathcal{H}^{F\,;(n)}_{ab}$ from the knowledge of $\hat{\sigma}^{\rm tot}_{F\,ab}$ at N$^{\rm n}$LO and of $d\hat{\sigma}^{(\rm fin.)}_{F\,ab}/dq_T^2$ at N$^{\rm n}$LO, without the need of explicitly computing the small-q_T behaviour of the spectrum $d\hat{\sigma}_{F\,ab}/dq_T^2$ at N$^{\rm n}$LO. For example, at exclusive N^{3}LO Eq. (30) reads

$$\begin{aligned}&\left(\frac{\alpha_S}{\pi}\right)^3\ \frac{M^2}{\hat{s}}\sum_c \sigma^{(0)}_{c\bar{c},\,F}(\alpha_S, M)\ \mathcal{H}^{F\,;(3)}_{c\bar{c}\leftarrow ab}\left(\frac{M^2}{\hat{s}};\frac{M^2}{\mu_R^2},\frac{M^2}{\mu_F^2},\frac{M^2}{Q^2}\right)\\ &= \left\{\left[\hat{\sigma}^{\rm tot}_{F\,ab}\right]_{\rm N^3LO} - \left[\hat{\sigma}^{\rm tot}_{F\,ab}\right]_{\rm NNLO}\right\} - \int_0^\infty dq_T^2\left\{\left[\frac{d\hat{\sigma}^{(\rm fin.)}_{F\,ab}}{dq_T^2}\right]_{\rm N^3LO} - \left[\frac{d\hat{\sigma}^{(\rm fin.)}_{F\,ab}}{dq_T^2}\right]_{\rm NNLO}\right\}\quad ,\end{aligned} \tag{36}$$

where $\alpha_S = \alpha_S(\mu_R^2)$ and we have used

$$\left[\hat{\sigma}^{\rm tot}_{F\,ab}(M,\hat{s};\alpha_S)\right]_{\rm LO} = \delta(1 - M^2/\hat{s})\ \sum_c \sigma^{(0)}_{c\bar{c},\,F}(\alpha_S, M)\ \delta_{ca}\ \delta_{\bar{c}b}\quad . \tag{37}$$

The generalization at any order n ($n > 1$) is [2]

$$\left(\frac{\alpha_S}{\pi}\right)^n \frac{M^2}{\hat{s}} \sum_c \sigma^{(0)}_{c\bar{c},\,F}(\alpha_S, M)\, \mathcal{H}^{F\,;(n)}_{c\bar{c}\leftarrow ab} = \left\{ \left[\hat{\sigma}^{\rm tot}_{F\,ab}\right]_{\rm N^nLO} - \left[\hat{\sigma}^{\rm tot}_{F\,ab}\right]_{\rm N^{n-1}LO} \right\} - \int_0^\infty dq_T^2 \left\{ \left[\frac{d\hat{\sigma}^{(\rm fin.)}_{F\,ab}}{dq_T^2}\right]_{\rm N^nLO} - \left[\frac{d\hat{\sigma}^{(\rm fin.)}_{F\,ab}}{dq_T^2}\right]_{\rm N^{n-1}LO} \right\}. \tag{38}$$

At LO, where only the Born subprocess is available, $\left[\frac{d\hat{\sigma}^{(\rm fin.)}_{F\,ab}}{dq_T^2}\right]_{\rm LO}$ is zero by definition. If all the components in right-hand side of Eq. (38) are known analytically (as it was the case at NNLO in Refs. [16, 17]) the function $\mathcal{H}^F_{ab}$ can be extracted exactly in analytical form. At NLO the extraction of the function $\mathcal{H}^{F\,;(1)}_{ab}$ is straightforward for Drell-Yan and Higgs boson production. The function $\mathcal{H}^{F\,;(2)}_{ab}$ at NNLO (for Higgs ($F = H$) boson production [16] and Drell-Yan ($F = DY$) [17]) can be obtained with a dedicated analytical computation using Eq. (38) for $n = 2$. Since for Higgs boson production, the transverse momentum cross section H+jet at NNLO is not known analytically, Eq. (36) can be used only numerically in the computation of the function $\mathcal{H}^{F\,;(3)}_{ab}$.

The following paragraphs will focus on the detailed degree of approximation that is intended to use. Instead of compute the entire third order function $\mathcal{H}^{H\,;(3)}_{ab}$ numerically (which is not recommended) we first report all its ingredients with the aim of reducing the numerical extraction to only a few components (perturbative functions).

The general structure of the coefficient $\mathcal{H}^{F\,;(3)}$ (which is proportional to $\delta(q_T^2)$) is not known in analytic form for any hard-scattering process. Nonetheless, within our subtraction formalism, $\mathcal{H}^{F\,;(3)}$ can be determined for any hard-scattering process whose corresponding total cross section is known at N^{3}LO.

At N^{3}LO the universal relation between $H^{F;(3)}_c$ and the third-order virtual correction to the partonic subprocess $c\bar{c} \to F$ presents one missing ingredient: the *single* coefficient (of *soft* origin) belonging to the finite part of the structure of the IR singularities, in the third-order virtual amplitude of the corresponding partonic subprocess $c\bar{c} \to F$. Although a general prescription to compute analytically the hard-virtual coefficient $H^{H;(3)}_g$ is not completely known, using the corresponding hard-virtual factor $C^{\rm th(3)}_{gg\to H}$ [30] for threshold resummation (in the large-m_t limit) and the exponential equation that relates threshold and q_T resummation hard-virtual coefficients

(Eq. (81) of Ref. [11]), we compute the following approximated expression

$$
\begin{aligned}
\widetilde{H}_g^{H;(3)} = C_A^3 \Bigg(&-\frac{15649\zeta_3}{432} - \frac{121\pi^2\zeta_3}{432} + \frac{3\zeta_3^2}{2} + \frac{869\zeta_5}{144} + \frac{215131}{5184} + \frac{16151\pi^2}{7776} - \frac{961\pi^4}{15552} + \frac{\pi^6}{810} \\
&+ \frac{105}{32}\zeta_6 \Bigg) + C_A^2 \left(\frac{605\zeta_3}{72} + \frac{55\pi^2\zeta_3}{36} + \frac{737\pi^2}{432} + \frac{167\pi^4}{432} + \frac{\pi^6}{72} \right) \\
&+ C_A \left(\frac{19\pi^2 L_t}{48} - \frac{55\pi^2\zeta_3}{8} - \frac{\pi^6}{480} + \frac{133\pi^4}{72} + \frac{11399\pi^2}{864} + \frac{63}{32}\zeta_6 \right) \\
&+ N_f^2 \Bigg(\frac{43 C_A\zeta_3}{108} - \frac{19\pi^4 C_A}{3240} - \frac{133\pi^2 C_A}{1944} + \frac{2515 C_A}{1728} - \frac{7 C_F\zeta_3}{6} \\
&+ \frac{4481 C_F}{2592} - \frac{\pi^4 C_F}{3240} - \frac{23\pi^2 C_F}{432} \Bigg) \\
&+ N_f \Bigg(\frac{101 C_A^2\zeta_5}{72} - \frac{97}{216}\pi^2 C_A^2\zeta_3 + \frac{29 C_A^2\zeta_3}{8} + \frac{1849\pi^4 C_A^2}{38880} - \frac{35\pi^2 C_A^2}{243} - \frac{98059 C_A^2}{5184} \\
&+ \frac{5 C_A C_F\zeta_5}{2} + \frac{13 C_A C_F\zeta_3}{2} + \frac{1}{2}\pi^2 C_A C_F\zeta_3 - \frac{63991 C_A C_F}{5184} + \frac{11\pi^4 C_A C_F}{6480} - \frac{71}{216}\pi^2 C_A C_F \\
&+ \frac{1}{9}\pi^2 C_A L_t - \frac{5}{36}\pi^2 C_A\zeta_3 - \frac{55 C_A\zeta_3}{36} - \frac{5\pi^4 C_A}{54} - \frac{1409\pi^2 C_A}{864} \\
&- 5 C_F^2\zeta_5 + \frac{37 C_F^2\zeta_3}{12} + \frac{19 C_F^2}{18} \Bigg) \ .
\end{aligned}
\tag{39}
$$

Notice that we neglect all the third order terms in the exponent of Eq. (81) in Ref. [11], considering the entire $\mathcal{O}(\alpha_S^3)$ correction (in the exponent) as unknown. The $\widetilde{H}_g^{H;(3)}$ coefficient in Eq. (39) will be used in the numerical computations in the present paper.

The missing terms in Eq. (39), concerning the final expression of $H_g^{H;(3)}$, have a *soft* origin. Following notation of Ref. [11], all the third order terms in the right hand side in Eq. (81) of Ref. [11] are denoted by $\delta_{(2)}^{q_T}$. This allows to perform a subsequent decomposition for the third order hard-virtual coefficient defined in Eq. (39)

$$
\widetilde{H}_g^{H;(3)} \equiv H_g^{H;(3)} - \left[H_g^{H;(3)}\right]_{(\delta_{(2)}^{q_T})} \ . \tag{40}
$$

Therefore the numerical extraction is constrained to the functions $G_{g\,a}^{(2)}(z)$, $C_{g\,a}^{(3)}(z)$ and $\left[H_g^{H;(3)}\right]_{(\delta_{(2)}^{q_T})}$. A naïve numerical implementation of Eq. (36) results in the following approximation

$$
\begin{aligned}
C_{N3}\ \ \delta_{g\,a}\,\delta_{g\,b}\,\delta(1-z)\ \leftarrow\ \ &\delta_{g\,a}\,\delta_{g\,b}\,\delta(1-z)\left[H_g^{H;(3)}\right]_{(\delta_{(2)}^{q_T})} + \delta_{g\,a}\,C_{g\,b}^{(3)}(z) + \delta_{g\,b}\,C_{g\,a}^{(3)}(z) \\
&+ \left(G_{g\,a}^{(1)} \otimes G_{g\,b}^{(2)}\right)(z) + \left(G_{g\,a}^{(2)} \otimes G_{g\,b}^{(1)}\right)(z) \ \ ,
\end{aligned}
\tag{41}
$$

where the third-order numerical coefficient C_{N3} embodies the numerical extraction of the hard-virtual coefficient $\left[H_g^{H;(3)}\right]_{(\delta_{(2)}^{q_T})}$ *plus* the numerical reduction of a function of the variable z to a numerical term proportional to $\delta(1-z)$. The resulting numerical coefficient $\left[H_g^{H;(3)}\right]_{(\delta_{(2)}^{q_T})}$ is exact since C_{N3} is proportional to $\delta(1-z)$. The approximation that implies Eq. (41) is related only to the functions $G_{g\,a}^{(2)}(z)$ and $C_{g\,a}^{(3)}(z)$, which their functional dependence on the variable z goes beyond terms proportional to $\delta(1-z)$.

The method proposed in Eq. (41) to approximate numerically unknown terms in the hard-virtual function $\mathcal{H}^{H}_{gg\leftarrow ab}(z)$ is not new. It was first used in Ref. [2] in order to compute numerically the second order function $\mathcal{H}^{H;(2)}_{gg\leftarrow ab}(z)$ at NNLO, providing a reasonable estimate of the exact result to better than 1% accuracy. Notice that Eq. (41) allows to recover the total cross section (at N^{3}LO in this case) with no approximation. After integration over the transverse momentum q_T, Eq. (29) provides the same total integral (numerically in this case) that in the fully analytical case. Even more, for IR safe observables (at fixed order) which verify that the *back-to-back* kinematical region ($q_T = 0$) is located in a single phase space point (e.g the q_T distribution, the angular separation $\Delta\Phi_{\gamma\gamma}$ between the two photons for a Higgs boson decaying into diphotons, etc.), we consider our fixed order result as with no approximation, i.e, the integral of the analytical unknown terms in Eq. (41) (which all have $q_T = 0$) are located in one single point of the exclusive differential distributions.

The precedent considerations about the approximation that proposes Eq. (41) were regarding the total cross section or differential distributions in which the Born–like configurations belong to one single phase space point. In order to quantify the quality of the approximation proposed in Eq. (41) at the differential level even when the Born differential cross section populates the entire differential range, we perform a detailed numerical study of the Higgs boson rapidity (y_H) in Sec. 4.1 at NNLO. This study can be performed only up to this perturbative order (NNLO) since all the required q_T subtraction ingredients are known analytically. We can anticipate our results saying that in the rapidity range $0 \leq y_H \leq 4$ the approximated NNLO result differs less than 0.2% respect to the exact NNLO Higgs rapidity distribution.

3.1 Implementation and setup of the numerical calculations

To extract the value of C_{N3}, we first introduce the numerical tools and the calculation setup in this section. We use the same setup throughout this paper also for the inclusive and differential predictions presented in Sections 3.2, 4.1, 4.2 and 4.3.

We consider the Higgs boson production in proton-proton collisions at the centre–of–mass energy $\sqrt{s} = 13$ TeV. In our computation we use the Higgs boson mass $M_H = 125$ GeV and the vacuum expectation value $v = 246.2$ GeV. The Born sub-process is initiated with gluon-gluon fusion mediated through a top quark loop. For Higgs production, which has a typical energy scale of M_H, it is possible to integrate out the top quark loop by taking the large-m_t limit ($m_t \to \infty$) and therefore, the Higgs boson is produced from the gluon-gluon-Higgs effective vertex [32]. The mass of the top quark is taken as $m_t = 173.2$ GeV in those contributions which do not vanish in the large-m_t limit (e.g Eqs. (45) and (39) and Wilson corrections at N^{3}LO). With the top quark loop replaced by an effective vertex, we consider a five-flavour scheme QCD with all light quarks being massless. We use the central set of the `PDF4LHC15` parton distribution functions (PDFs) [33] as implemented in the `LHAPDF` framework [34] and the associated strong coupling constant $\alpha_S(M_Z) = 0.118$. Notice that we systematically employ the same order of the PDFs (NNLO) for the LO,NLO,NNLO and N^{3}LO results presented in this paper. The default factorization and renormalization scales are chosen accordingly as $\mu \equiv \mu_R = \mu_F = M_H/2$. The theoretical uncertainty is estimated by varying the default scale choice independently for μ_R and μ_F by a factor of $\{1/2, 2\}$ while omitting combinations of $\mu_R/\mu_F = 4$ or $1/4$ which result in seven-point scale variation choices.

As stated in Sec. 3 and in Refs. [1, 2], the computation of the total cross section or differential distributions under the q_T subtraction formalism can be separated into two main parts by inserting Eq. (31) into Eq. (30):

$$\hat{\sigma}^{\rm tot}_{F\,ab} = \left[\frac{M^2}{\hat{s}}\,\mathcal{H}^F_{ab} - \int_0^\infty dq_T^2\,\frac{d\hat{\sigma}^{F\,\rm CT}_{ab}}{dq_T^2} \right] + \int_0^\infty dq_T^2\,\frac{d\hat{\sigma}^{F+\rm jets}_{ab}}{dq_T^2} \quad . \tag{42}$$

Regarding the $d\hat{\sigma}^{F+\rm jets}_{ab}$ contribution in Eq. (42), we make use of the parton-level event generator `NNLOJET` which provides the necessary infrastructure for the antenna subtraction method up to NNLO [7]. This program performs the integration of all contributing subprocesses of the type $d\hat{\sigma}^{F+\rm jets}_{ab}$ as well as the convolution with PDFs at this order. Processes at NNLO with the structure of $d\hat{\sigma}^{F+\rm jets}_{ab}$ implemented in `NNLOJET` are: $F = H$ [35, 36], $F = Z$ [37, 38, 39] and $F = W^\pm$ [39]. In this paper we only focus in the study of $F = H$ but the formalism could be easily extended to Z and $W^\pm$.

The q_T counter term and the hard function $\mathcal{H}^F$ (terms in square bracket in Eq. (42)), are encoded in a new Monte Carlo generator `HN3LO` up to the third order in the strong coupling constant. After expanding Eq. (7) to this order, several non-trivial convolutions emerge and we document the corresponding formulae implemented in `HN3LO` in Appendix A. All our results up-to the NNLO are in accord with the Monte Carlo generator `HNNLO` [1] at the per mille level of accuracy. In the right hand side of Eq. (36), the partonic Higgs boson total cross sections at NNLO ($\left[\hat{\sigma}^{\rm tot}_H\right]_{\rm NNLO}$) and N^{3}LO ($\left[\hat{\sigma}^{\rm tot}_H\right]_{\rm N^3LO}$) are also required. We consider the analytical total Higgs boson cross section at N^{3}LO $\left[\sigma^{\rm tot}_H\right]_{\rm N^3LO}$ (i.e $\left[\hat{\sigma}^{\rm tot}_H\right]_{\rm N^3LO}$ convoluted with the PDFs) calculated recently in Ref. [40] and we employ the numerical code `ihixs 2` (see Ref. [41]) to compute not only the N^{3}LO cross section, but also, any of the analytical total cross sections used (and required) to compute the missing coefficient C_{N3}.

The numerical computation of the integral of the difference $d\sigma^{F+\rm jet}_{\rm NNLO} - d\sigma^{F\,\rm CT}_{\rm N^3LO}$ in Eq. (31), although finite, requires the implementation of a suitable technical lower bound or q_T^{cut}. This technical cut introduces systematic uncertainties to both $d\sigma^{F+\rm jet}_{\rm NNLO}$ and $d\sigma^{F\,\rm CT}_{\rm N^3LO}$. With proper cancellations between the terms on the right hand side of Eq. (42), the corresponding numerically calculated total cross sections and differential distributions have to result q_T^{cut} independent (within the statistical errors) in some domain of the transverse momentum which contains the chosen value of q_T^{cut}. Therefore there is an interplay between the q_T^{cut} value and the statistical and systematics uncertainties of the resulting cross section. As q_T^{cut} in going to zero (as well as the the systematic uncertainties) the numerical fluctuations start to grow due to the cancellation of two opposite large cross sections and due to large dynamical range involved in $d\sigma^{F+\rm jet}_{\rm NNLO}$. The numerical stability of $d\sigma^{F+\rm jet}_{\rm NNLO}$ at small q_T using `NNLOJET` has been systematically validated for Higgs (with $q_T^{cut} = 0.7$ GeV in Ref. [25]) and Drell-Yan (with $q_T^{cut} = 2$ GeV in Ref. [26]) production at the LHC. In Sections 3.2, 4.1, 4.2 and 4.3, we document numerical results combined with q_T subtraction formalism using $q_T^{cut} = (2 \pm 1)$ GeV.

3.2 The numerical computation of C_{N3}

Now we turn the discussion to the numerical results regarding the extraction of C_{N3} coefficients and the corresponding N^{3}LO total cross sections.

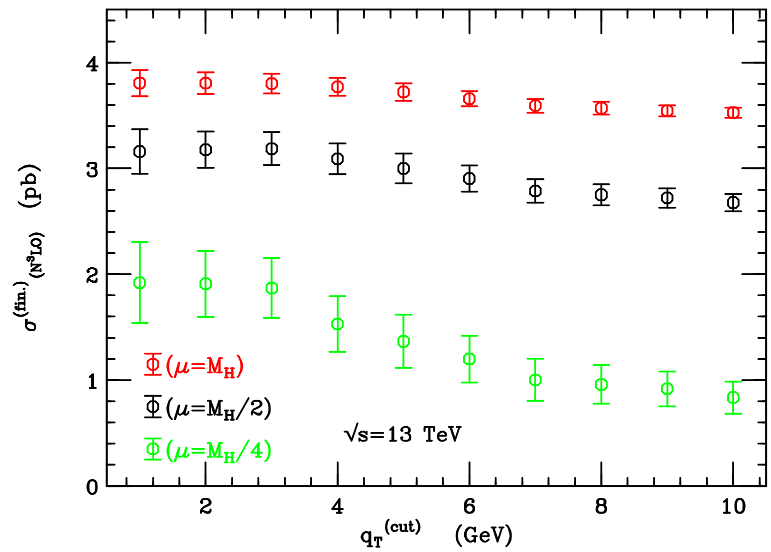

Figure 1: *The q_T integrated finite contribution to the cross section of Eq. (31) at N^{3}LO exclusively (i.e N^{3}LO-NNLO) between $q_T^{\rm cut}$ and ∞, for three different scales ($\mu = \mu_R = \mu_F$).*

In Fig. 1 we report the $\sigma^{(\rm fin.)}_{F=H}$ (i.e $\hat{\sigma}^{(\rm fin.)}_H$ convoluted with the parton distribution functions) cross section at N^{3}LO exclusively as a function of the $q_T^{\rm cut}$. With N^{3}LO exclusively we understand $\left[\sigma_H^{(\rm fin.)}\right]_{\rm N^3LO} - \left[\sigma_H^{(\rm fin.)}\right]_{\rm NNLO}$. Using Eq. (35) with Eq. (36) and the value of the resulting integral $\sigma_H^{(\rm fin.)}(q_T^{\rm cut} = 1$ GeV) in Fig. 1, it is possible to obtain the q_T integrated cross section of the unknown terms in the right hand side of Eq. (41) and consequently C_{N3}.

The behaviour of the N^{3}LO $\sigma_H^{(\rm fin.)}$ cross section as a function of $q_T^{\rm cut}$ in Fig. 1 allows also to estimate the systematical uncertainty corresponding to the use of this technical cut which turns out to be at the *per mille* level in the domain $q_T^{cut} = (2 \pm 1)$ GeV. More clearly, variations of the $q_T^{\rm cut}$ parameter from $q_T^{\rm cut} = 1$ GeV to 3 GeV produce variations in the resulting $\sigma_H^{(\rm fin.)}$ cross section of the order of the 0.1%.

In Fig. 2 we show the C_{N3} predicted value for each scale (in black points). Notice that the central value of each predicted C_{N3} is independent of the scale (within the uncertainties), in complete agreement with Eq. (35). The scale independence of C_{N3} is not related with the used ansatz of Eq. (41). The terms in the right-hand side of Eq. (35) are all scale independent and the relation between C_{N3} and $\widetilde{H}_g^{H;(3)}$ is univocal defined considering Eqs. (35), (40) and (41). The black error bars for each one of the C_{N3} values are calculated with the conventional propagation of the uncertainties and it is almost entirely due to the size of the statistical uncertainties of the N^{3}LO $\sigma_H^{(\rm fin.)}$ cross section in Fig. 1.

The solid red central line in Fig. 2, is the average value calculated with the three different central black points corresponding to each scale choice, whereas the red band is the predicted uncertainty. The uncertainty is estimated considering the average of the three largest (smallest) values for the C_{N3} coefficient resulting after adding (subtracting) the corresponding statistical uncertainty at each scale. The value of the resulting coefficient using the three scales presented in Fig. 2 is $C_{N3} = -932 \pm 224$. Besides the precedent cited three central scales we also present

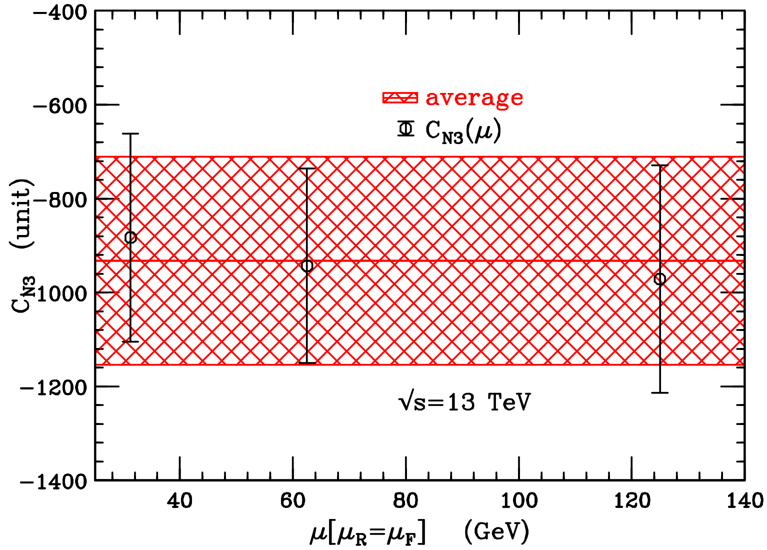

Figure 2: *The numerically computed C_{N3} coefficient as defined in Eq. (41) (black points) for the particular case of $q_T^{cut} = 1$ GeV. The black error bars for each C_{N3} point is obtained propagating the statistical uncertainties of the different terms involved in the computation. The red band is calculated with the average of the three particular C_{N3} values for each scale as detailed in the text.*

predictions for other four scales that complete a seven–point scale choice varying the default scale ($M_H/2$) by a factor $\{1/2, 2\}$. In Fig. 3 we show the computed C_{N3} coefficients corresponding to each one of the seven scales as a function of the label of the scale as stated in Table 1. The red band and central value (red line) is calculated with the first three black points at $q_T^{cut} = 1$ GeV already present in Fig. 2 and detailed in Table 1 in bold typeface. In Fig. (3) we also compare the computed C_{N3} coefficients at $q_T^{cut} = 1$ GeV with the cases in which $q_T^{cut} = 2$ GeV (blue points) and 3 GeV (green points) are used. The variation of the q_T^{cut} around 2 GeV quantifies the stability of the C_{N3} extraction. The central value for the C_{N3} coefficient was obtained only using the three central scales $\mu = M_H, M_H/2, M_H/4$ since the other four scales, which are correlated with the previous, does not aport new and independent information to the average. Even more, considering in the average the seven scales, this will result in a shift of -30 units in the central value of C_{N3}, which at the level of the total cross sections (at each scale) represents less than the 0.1%. Regarding the estimation of the uncertainty in the computation of C_{N3}, considering the seven scales, it leaves without changes this value. In Sec. 4.2 we will estimate how affect the uncertainty associated to the C_{N3} parameter, the differential distributions.

Whereas the C_{N3} coefficient is independent of the scale choice, its resulting cross section, after convolution with the PDFs (which depend on μ_F) and the strong coupling constant $\alpha_S(\mu_R)$, does depend on the scale choice. In Table 1 we present all the C_{N3} coefficients as a function of the scale choice and the q_T^{cut} ($q_T^{cut} = 2 \pm 1$ GeV).

The numerically calculated C_{N3} coefficient allows to predict the total cross section at N^{3}LO within the transverse momentum subtraction method (as well completely differential distributions). In Fig. 4 we compare the fully analytical N^{3}LO Higgs boson total cross section [40] (black points) and our best estimation (green points) for three central scales, using $q_T^{cut} = 1$ GeV. The blue squared points constitute our best approximation without the use of the C_{N3} coefficient (i.e

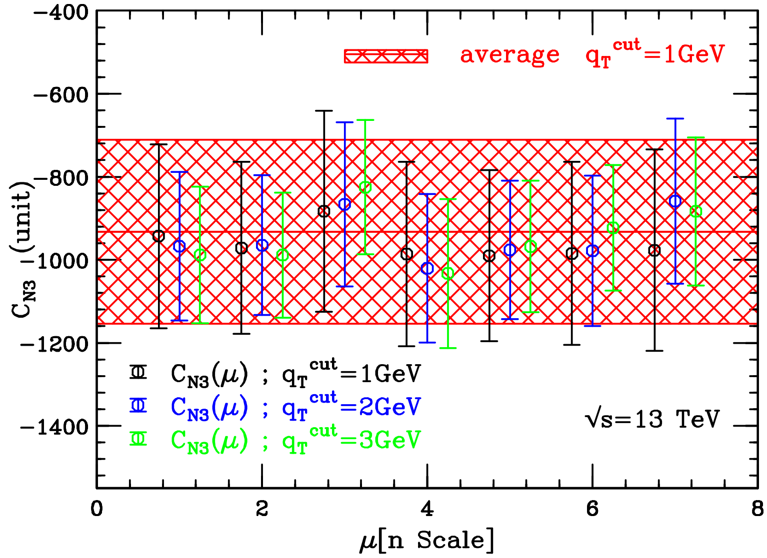

Figure 3: *The numerically computed C_{N3} coefficient (for three different values of q_T^{cut}) as a function of the number of the scale as detailed in Table 1. The error bars for each particular C_{N3} point is obtained propagating the statistical uncertainties of the different terms involved in the computation. The red band is calculated with the average of the three particular C_{N3} values of the three scales present in Fig. 2 at $q_T^{cut} = 1$ GeV, as detailed in the text.*

$C_{N3} = 0$), that can be consider as the prediction of the q_T subtraction method in the case in which the total cross section is unknown (e.g for Drell-Yan at N^{3}LO). The uncertainty bars in the q_T subtraction prediction correspond to the statistical errors of the numerical computations and are mainly due to the finite contribution in Eq. (31) at N^{3}LO exclusively. The magenta and cyan points correspond to our N^{3}LO prediction using $q_T^{cut} = 2$ GeV and 3 GeV respectively. Notice that the q_T^{cut} variation is performed at N^{3}LO exclusively, while the NNLO cross section is not varied over the different q_T^{cut} parameters. The NNLO cross section is also shown in Fig. 4 (red star points) in order to put in evidence the size of the N^{3}LO corrections respect to the precedent perturbative order. The total cross sections shown in Fig. 4 are explicitly reported in Table 2.

4 The rapidity distribution of the Higgs boson

In this section we use the C_{N3} coefficient (computed in Sec. 3.2) to produce differential predictions at N^{3}LO. In particular we present differential results for the rapidity distribution of the Higgs boson. In Sec. 4.1 we estimate at NNLO the uncertainties introduced in the rapidity distribution, by the procedure proposed in Eq. (41). In Sec. 4.2 we present the rapidity distribution at N^{3}LO with the corresponding estimation of the uncertainties associated to the variation of the $q_T^{\rm cut}$ and C_{N3} parameters.

n	$\left[\tilde{\mu_R}, \tilde{\mu_F}\right] \times M_H$	C_{N3} ($q_T^{\rm cut} = 1$ GeV)	C_{N3} ($q_T^{\rm cut} = 2$ GeV)	C_{N3} ($q_T^{\rm cut} = 3$ GeV)
(1)	$\left[1/2, 1/2\right]$	$\mathbf{-943 \pm 222}$	-967 ± 179	-988 ± 164
(2)	$\left[1, 1\right]$	$\mathbf{-971 \pm 207}$	-965 ± 168	-989 ± 151
(3)	$\left[1/4, 1/4\right]$	$\mathbf{-883 \pm 243}$	-866 ± 198	-850 ± 162
(4)	$\left[1/2, 1\right]$	-986 ± 222	-1021 ± 179	-1033 ± 179
(5)	$\left[1, 1/2\right]$	-990 ± 206	-976 ± 167	-968 ± 158
(6)	$\left[1/2, 1/4\right]$	-985 ± 221	-978 ± 181	-923 ± 152
(7)	$\left[1/4, 1/2\right]$	-977 ± 243	-859 ± 199	-883 ± 179

Table 1: *Predicted values of the C_{N3} coefficients as a function of the q_T^{cut} as shown in Fig. 3 for each scale choice (second column). In bold typeface the C_{N3} coefficients (for the case q_T^{cut} =1 GeV) which are used to compute the averaged value $C_{N3} = -932 \pm 224$ shown in Figs. 2 and 3, with the central red line and the corresponding red band. The uncertainty for each one of the C_{N3} coefficients is calculated with the customary propagations of the uncertainties. The first column is used to label each particular scale choice used in Fig. 3.*

$\sigma_H^{\rm tot}$ (pb)	Exact	q_T subtraction ($q_T^{\rm cut} = 1$ GeV)	q_T subtraction ($q_T^{\rm cut} = 2$ GeV)	q_T subtraction ($q_T^{\rm cut} = 3$ GeV)	q_T subtraction ($C_{N3} = 0$)
$\rm N^3LO$ $[\mu = M_H/2]$	44.97	44.98 ± 0.21	45.00 ± 0.17	45.02 ± 0.15	45.86 ± 0.21
$\rm N^3LO$ $[\mu = M_H]$	43.50	43.52 ± 0.12	43.52 ± 0.10	43.53 ± 0.09	44.08 ± 0.12
$\rm N^3LO$ $[\mu = M_H/4]$	45.06	44.98 ± 0.38	44.96 ± 0.31	44.93 ± 0.28	46.44 ± 0.38
NNLO $[\mu = M_H/2]$	43.47	43.46 ± 0.02	43.46 ± 0.02	43.46 ± 0.02	43.46 ± 0.02
NNLO $[\mu = M_H]$	39.64	39.62 ± 0.02	39.62 ± 0.02	39.62 ± 0.02	39.62 ± 0.02
NNLO $[\mu = M_H/4]$	47.33	47.33 ± 0.02	47.33 ± 0.02	47.33 ± 0.02	47.33 ± 0.02

Table 2: *The total cross section for Higgs boson production $\sigma_H^{\rm tot}$ at the LHC ($\sqrt{s} = 13$ TeV). Results for NNLO and N^{3}LO cross sections for three different scales $\mu = M_H/2$ (central scale), $\mu = M_H$ and $\mu = M_H/4$. The column "Exact" contains the results of Ref. [40] computed with the numerical code of Ref. [41] as detailed in the text. The results with the q_T subtraction method are obtained using three different values of $q_T^{\rm cut}$ (1,2 and 3 GeV), and their uncertainties are calculated with the customary propagation of statistical errors. The last column shows $\sigma_H^{\rm tot}$ obtained with the q_T subtraction method and using $C_{N3} = 0$ at N^{3}LO. The values of $\sigma_H^{\rm tot}$ reported in this Table are shown in Fig. 4. The NNLO cross sections computed with the q_T subtraction method are obtained using $q_T^{\rm cut} = 1$ GeV, i.e, the variation of this parameter in the N^{3}LO cross section is considered only at N^{3}LO exclusively.*

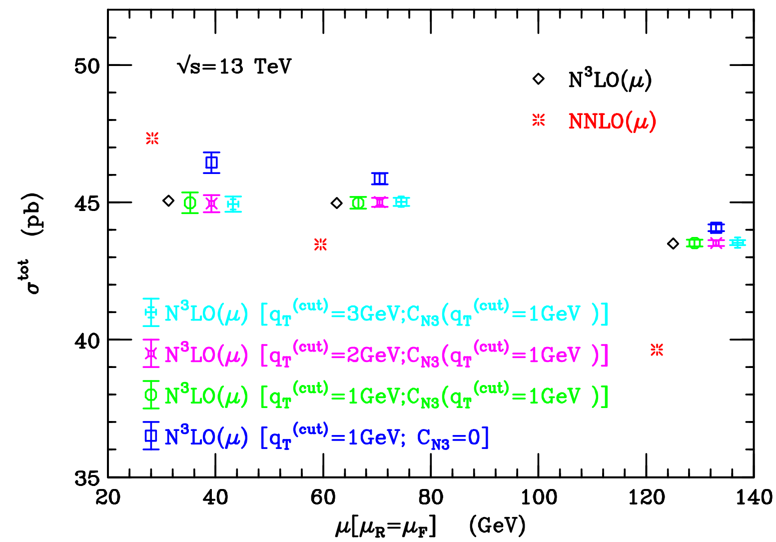

Figure 4: *Total cross section of Higgs boson production, $\left[\sigma_H^{\rm tot}\right]_{\rm N^3LO}$, as predicted by the q_T subtraction formalism, compared with the corresponding analytical $\left[\sigma_H^{\rm tot}\right]_{\rm N^3LO}$ of Ref. [40] (black diamonds). In green points we present the q_T subtraction prediction for q_T^{cut}=1 GeV. In magenta points we consider $\left[\sigma_H^{\rm tot}\right]_{\rm N^3LO}$ but using q_T^{cut}=2 GeV, and in cyan the corresponding cross section using q_T^{cut}=3 GeV. Whereas the q_T^{cut} is changed (from 1 to 3 GeV) the coefficient C_{N3} is always considered the same (as calculated in Fig. 2 for q_T^{cut}=1 GeV). The q_T subtraction prediction at N^{3}LO with the C_{N3} numerical coefficient fixed to zero (using q_T^{cut}=1 GeV) is shown with blue squared points. The NNLO analytical Higgs boson cross section ($\left[\sigma_H^{\rm tot}\right]_{\rm NNLO}$) is presented in pink star points. All the cross sections are shown for three different scales: $\mu \equiv \mu_R = \mu_F = \{1/4, 1/2, 1\}M_H$. The uncertainty bars in the q_T subtraction predictions are calculated with the customary propagation of statistical uncertainties.*

4.1 The NNLO rapidity distribution

In this section we quantify the uncertainty in the approximation proposed in Eq. (41) but at NNLO. This approximation was first proposed in Ref. [2] for Higgs production at NNLO. Now since all the ingredients of the q_T subtraction formalism at NNLO are known, it is possible to evaluate the deviation caused by the approximation from the exact result. This analysis provide related information about how much the deviation from the exact result could be at N^{3}LO in Sec. 4.2 and 4.3. For the present quantitative exercise we take as known the collinear functions $C^{(1)}_{g\,a}$ and the hard-virtual factor $H_g^{H;(1)}$ in Eq. (34). The collinear functions $C^{(2)}_{g\,a}$ and the first order helicity-flip functions $G^{(1)}_{g\,a}$ are regarded as unknown. The hard-virtual factor $H_g^{H;(2)}$ is divided in two contributions as in Eq. (40)

$$\widetilde{H}_g^{H;(2)} \equiv H_g^{H;(2)} - \left[H_g^{H;(2)}\right]_{(\delta^{q_T}_{(1)})} , \tag{43}$$

where $\left[H_g^{H;(2)}\right]_{(\delta^{q_T}_{(1)})}$ is considered as unknown for the present NNLO study. The so called *unknown functions* (for this exercise) which depend on the variable z in Eq. (34) are approximated with a single numerical coefficient C_{N2} proportional to $\delta(1-z)$ (the C_{N2} here was labeled as C_N in

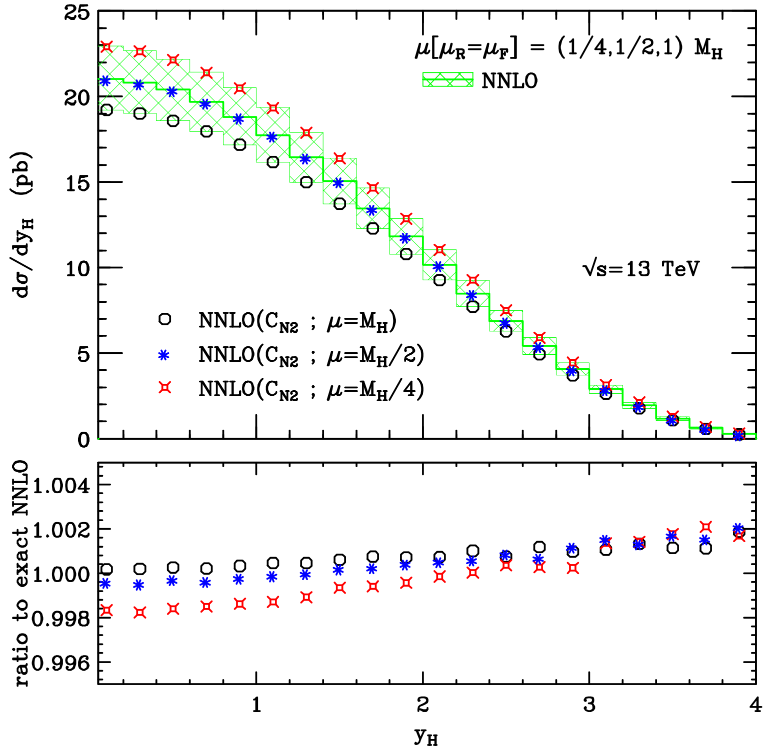

Figure 5: *Rapidity distribution at NNLO predicted by the q_T subtraction formalism (solid green band) compared with the prediction using the C_{N2} numerical coefficient (red, blue and black points). In the lower panel we show the ratio to the exact NNLO result. For this particular example at NNLO, we employ the three points scale variation: $\mu = \mu_R = \mu_F = \{M_H/4, M_H/2, M_H\}$.*

Ref. [2])

$$C_{N2} \;\; \delta_{g\,a}\,\delta_{g\,b}\,\delta(1-z) \;\leftarrow\; \delta_{g\,a}\,\delta_{g\,b}\,\delta(1-z)\left[H_g^{H;(2)}\right]_{(\delta_{(1)}^{q_T})} \\ +\delta_{g\,a}\,C_{g\,b}^{(2)}(z)+\delta_{g\,b}\,C_{g\,a}^{(2)}(z)+\left(G_{g\,a}^{(1)}\otimes G_{g\,b}^{(1)}\right)(z) \;\; . \tag{44}$$

In Fig. 5 we show the rapidity distribution of the Higgs boson at NNLO computed with the exact q_T subtraction (green band) and the NNLO prediction using the C_{N2} coefficient (red, blue and black points). For this particular example at NNLO, we employ the three–point scale variation: $\mu = \mu_R = \mu_F = \{M_H/4, M_H/2, M_H\}$. Repeating the analysis performed for the completion of Table 1, and Fig. (2) we arrive to the following result: $C_{N2} = 28 \pm 1$. The numerical value of the C_{N2} parameter corresponds to a specific $\widetilde{H}_g^{H;(2)}$ hard coefficient:

$$\widetilde{H}_g^{H;(2)} = \frac{11399}{144} + \frac{19}{8}L_t - \frac{1189}{144}N_f + \frac{2}{3}N_f L_t + \frac{83}{6}\pi^2 - \frac{5}{18}\pi^2 N_f + \frac{13}{16}\pi^4 - \frac{165}{4}\zeta_3 + \frac{5}{6}N_f\zeta_3 \;\; , \tag{45}$$

which is obtained with the same method that was used to arrive to Eq. (39). Using this C_{N2} parameter we can produce differential predictions which are obtained *mimicking* the strategy that we intend to use at N^3LO.

In the lower panel of Fig. 5 we show the ratio to the exact NNLO result, i.e we present the ratio for each scale. As expected, the approximation presents its best behaviour at central rapidity and the deviation from the exact results is at *per mile* level throughout the presented rapidity region of $|y_H| \leq 4$.

The numerical implementation of the q_T subtraction method (more precisely Eq. (38) at NNLO) requires the implementation of a lower technical cut ($q_T^{\rm cut}$) in the integral performed over the transverse momentum of the finite contribution in Eq. (31). The computation of the NNLO Higgs boson cross section and differential distributions do not represent a technical challenge, and the $q_T^{\rm cut}$ can be considered as low as the computation demands. We performed variations of the $q_T^{\rm cut}$ between 0.1 GeV and 3 GeV, and the NNLO cross sections (and differential distributions) present deviations within a 0.5% level of accuracy (the largest deviation 0.5% is always manifested for the scale choice $\mu = M_H/4$).

4.2 Numerical stability of the N^{3}LO rapidity distribution

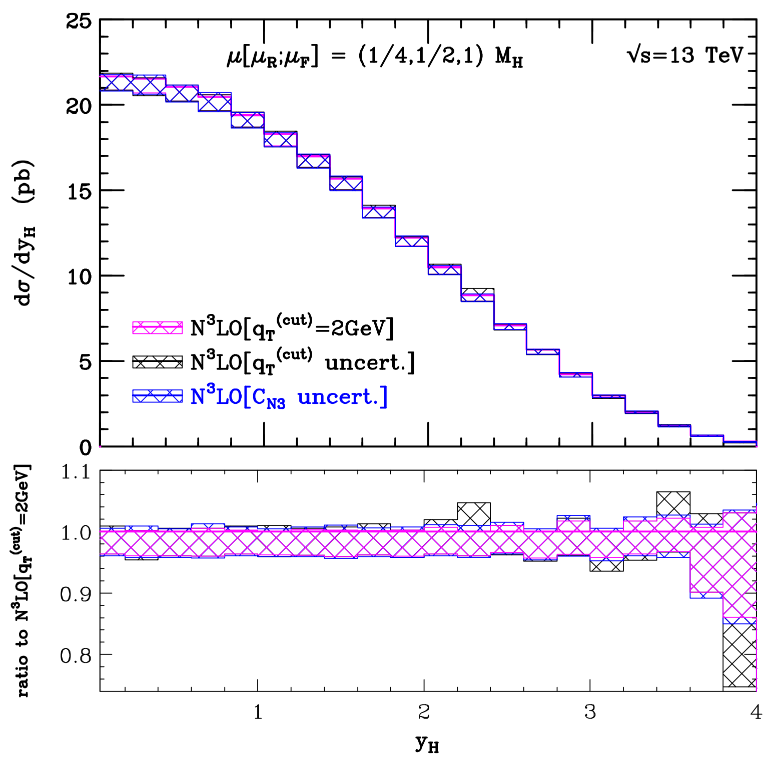

Figure 6: *Rapidity distribution of the Higgs boson as predicted by the q_T subtraction formalism at N^{3}LO. The bands are the result of the variation of the scales at seven–point as detailed in Table 2. The magenta band constitutes our prediction using $q_T^{\rm cut} = 2$ GeV using the central value for the C_{N3} coefficient ($C_{N3} = -932$). The black band is obtained as the envelope between the prediction at $q_T^{\rm cut} = 1$ GeV and 2 GeV using $C_{N3} = -932$. The blue band is computed taking the two extremal values of the C_{N3} coefficient for each one of the seven scales accordingly to the calculated uncertainty ($C_{N3} = -932 \pm 224$) for this third order coefficient as described in the text.*

In this section, we quantify the numerical stability (as well the involved intrinsic uncertainties) of the Higgs boson rapidity distributions at N^{3}LO regarding the $q_T^{\rm cut}$ and C_{N3} parameters and the statistical uncertainties introduced by $d\sigma^{(\rm fin.)}_{F=H}/dy_H$ at exclusive N^{3}LO.

In Fig. (6) we show the rapidity distribution at N^{3}LO obtained with the q_T subtraction method using the C_{N3} coefficient calculated in Sec. 3.2 ($C_{N3} = -932 \pm 224$). The magenta band in Fig. (6) is computed using $q_T^{\rm cut} = 2$ GeV and performing the seven–point scale variation specified in Table 2. The black band is calculated as the envelope of the rapidity bands for two different values of $q_T^{\rm cut}$ (1 GeV and 2GeV). Therefore, the black band in Fig. (6) can be taken as the estimation of the uncertainty due to the implementation of different $q_T^{\rm cut}$ parameters at N^{3}LO exclusively. The NNLO prediction is always computed with $q_T^{\rm cut} = 1$ GeV. In Fig. (4) (and also in Table 2), the total cross section (for the three central scales) is rather stable as a function of the $q_T^{\rm cut}$. The variations of the N^{3}LO cross sections are at the *per mille* level of accuracy if we consider $q_T^{\rm cut} = 2 \pm 1$ GeV, which is far better than the associated statistical uncertainty (see Table 2). The estimation of the uncertainty due to the $q_T^{\rm cut}$ variation performed in Fig. (6) (which is differential in the rapidity of the Higgs boson) confirms the stability of the total cross section reported in Table 2. This reported stability of the total cross section regarding the variation of the $q_T^{\rm cut}$ parameter was previously presented in Fig. (1) when the the behaviour of the q_T integrated finite contribution was shown as a function of the $q_T^{\rm cut}$.

The rapidity is almost insensitive to the change in the $q_T^{\rm cut}$ parameter where the bulk of the cross section takes place ($|y_H| \leq 3.6$). At large rapidities ($|y_H| \sim 4$), where the contribution to the total cross section is less than 0.5%, we found the largest deviations. Such deviation is related to the numerical uncertainties from $d\sigma^{(\rm fin.)}_{F=H}/dy_H$ at exclusive N^{3}LO which presents a very limited number of parton events, due to the much smaller event weight at large y_H.

Finally, we consider the uncertainty introduced by the statistical errors of the C_{N3} coefficient. The blue band in Fig. (6) is obtained as the envelope of the seven scales variation at $q_T^{\rm cut} = 2$ GeV now considering for each scale the two extremal C_{N3} coefficients corresponding to its maximum and minimum statistical deviations: $C_{N3} = (-1156, -708)$. Therefore the envelope is taken making use of 14 rapidities distributions (two extremal predictions for each one of the seven scales). The net effect of this C_{N3} variation result in an overall enlargement of the customary magenta band at $q_T^{\rm cut} = 2$ GeV. Our final estimation of the uncertainties in the rapidity of the Higgs boson at N^{3}LO is computed as the envelope of three bands: the band originated from the $q_T^{\rm cut} = 1$ GeV, the corresponding band containing both, the seven scales variation and the estimation of the C_{N3} statistical uncertainty and our best prediction for $q_T^{\rm cut} = 2$ GeV.

4.3 The rapidity distribution of the Higgs boson at N^{3}LO

In this section we present our predictions for the Higgs boson rapidity distributions at the LHC, applying the N^{3}LO q_T subtraction method presented in Sec. 2. The setup of the calculation was stated in Sec. 3.2. In Fig. 7 we show the rapidity distribution of the Higgs boson at LO (dashed black band), NLO (blue solid band), NNLO (green solid band) and N^{3}LO (magenta solid band). The N^{3}LO band is computed taking into account the uncertainties due to $q_T^{\rm cut}$ and C_{N3} as explained in Sec. 4.2.

The central scale ($\mu = M_H/2$) is shown with a solid line while the variation of the scales by a factor $\{1/2, 2\}$ producing the seven–point scale variation band. It is interesting to notice that from LO to NNLO, the scale $\mu = M_H/2$ is always at the center of the corresponding scale variation band in Fig. 7. At N^{3}LO the central scale $\mu = M_H/2$ (magenta solid line) almost coincides with the limit of the upper band. The precedent fact is the differential manifestation of what was shown in Fig. 4 for the total cross section: for $\mu = M_H/4$ and $\mu = M_H/2$ the total N^{3}LO cross sections are in accord at the 0.2% level (see Table 2 and Fig. (4)), noticing that the scale $\mu = M_H/4$ is at the top of the scale variation band for the whole rapidity range. Figs. 4 and 7 show a substantial reduction in the size of the variation of the scales at N^{3}LO, in the total cross section and in differential distributions, respectively.

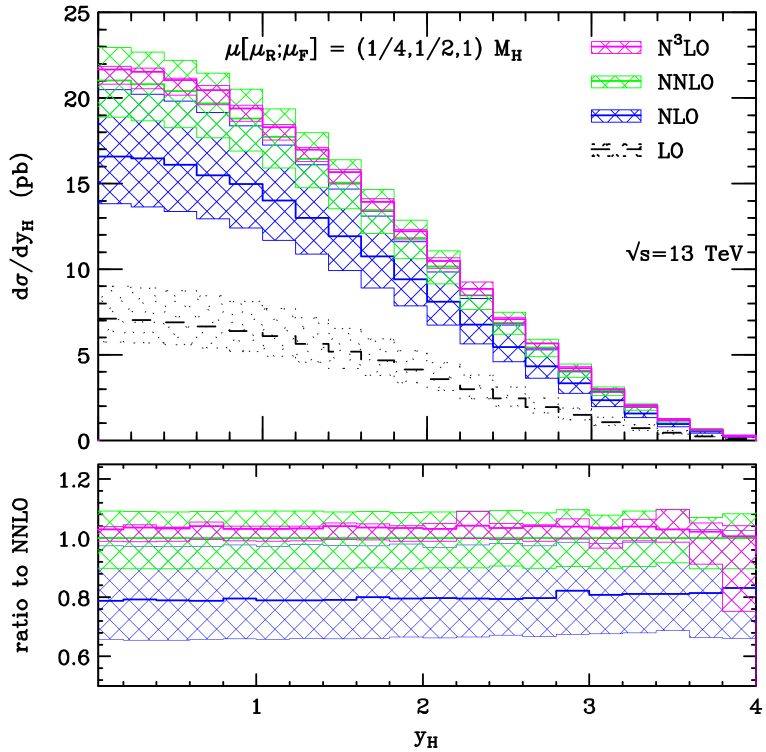

Figure 7: *Rapidity distribution of the Higgs boson as predicted by the q_T subtraction formalism up to N^{3}LO. The seven–point scale variation bands (as stated in Table 1) of the LO, NLO, NNLO and N^{3}LO(C_{N3}) results are as follows: LO (black dashed), NLO (blue solid), NNLO (green solid) and N^{3}LO(C_{N3}) (magenta solid). The central scale ($\mu = M_H/2$) at each perturbative order, is shown with solid lines respecting the colour of the corresponding perturbative order. In the lower panel, the ratio to the NNLO prediction is shown. While the bands for the predictions at LO, NLO and NNLO are computed with the seven scales as detailed in the text, the N^{3}LO(C_{N3}) band is obtained after considering also the uncertainties due to the variation of the q_T^{cut} and the C_{N3} coefficient.*

In the central rapidity region of $|y_H| \leq 3.6$, the impact of the N^{3}LO corrections on the NNLO result is almost independent of y_H with a flat k factor about 1.035 for the central scale choice. The combined theoretical uncertainty at N^{3}LO is at most of $\pm 5\%$ level with respect to the central scale choice. The precision of y_H distribution is improved by more than 50% from NNLO to N^{3}LO. The N^{3}LO theoretical uncertainty band stays within the scale variation band of NNLO except for the very large rapidity region.

Comparing Fig.(7) with previous results from the expansion of analytic N^{3}LO coefficient functions around the production threshold of the Higgs boson [6], although with different choices of PDFs and scale variation regions, the central scale results of the rapidity region $y_H < 0.5$ agree well between the two calculations. Both calculations demonstrate considerable reduction for the scale variation band from NNLO to N^{3}LO at central rapidity region. For the rapidity region $y_H > 1$, the current q_T subtraction formalism at N^{3}LO present different results compare to threshold expansion with the first two orders at N^{3}LO that the scale variation band for N^{3}LO staies outside the corresponding one at NNLO. This indicates a combined effect for having C_{N3} approximation in one calculation while the missing higher order terms from threshold expansion are sizable for the other calcualtion.

5 Conclusions and outlook

In this paper we have made a detailed study of Higgs boson production at the LHC using the q_T subtraction formalism at N^{3}LO. We systematically study the q_T subtraction formalism using hard resummation scheme for a generic colourless and massive system $F(\{q_i\})$ produced in hadron colliders. Fully differential cross sections of this type of final state system are factorized into $\delta(q_T)$ and $q_T \neq 0$ contributions. The contribution for $q_T \neq 0$ is calculated by the difference between $F(\{q_i\})$+jets framework and q_T counter terms. Specifically for N^{3}LO Higgs production, we use the `NNLOJET` package which contains the NNLO Higgs plus jet framework and expand the Sudakov from factor under hard resummation scheme to the matching order for the corresponding q_T counter terms. The contribution at $\delta(q_T)$ is further factorized into convolutions of Sudakov form factor, hard-virtual function, helicity-flip coefficient function, hard-collinear coefficient function as well as parton-distribution function (Sec.2). The factorization under hard resummation scheme guarantees all the process dependent contributions proportional to a form factor are included in the hard-virtual function which depends on both initial and final state particles. All other factorized contributions only depend on initial states. Some of the factorized ingredients contributing at $\delta(q_T)$ are not analytically known at N^{3}LO for the moment. We collect all analytically available contributions and approximate the unknown pieces by a constant coefficient C_{N3} which is scale and process independent (Sec.3). Using the available inclusive total cross section for N^{3}LO Higgs production and the known pieces from q_T subtraction formalism, we numerical abstract the value of C_{N3}. By comparing the numerical results of C_{N3} from different scale and q_T^{cut} setups during the abstraction, we conclude with very consistent results that C_{N3} is independent of the scale choices and the averaged value is $C_{N3} = -932 \pm 224$ (Sec.3.2).

As a prove of concept calculation using q_T subtraction method at N^{3}LO, with all the ingredients either analytically or numerically available, we calculate the total cross section and rapidity distributions for Higgs boson production at LHC using a new Monte Carlo generator `HN3LO`. Using the same averaged value of C_{N3}, we produce the inclusive total cross section in three different scale choices and find excellent agreement with the exact results (from `ihixs 2` [41]) at 0.02% level of accuracy for all three scales. For differential rapidity distribution of the Higgs boson, we first study the systematic error in analog of the C_{N3} approximation but at NNLO by introducing C_{N2}. The NNLO y_H distributions are at per mile level agreement between the C_{N2} approximation and the exact results. With the approximation at NNLO proved to be reliable, we calculate, with seven–point scale variations, the y_H distribution at N^{3}LO including also systematic errors regarding different q_T^{cut} and C_{N3} values. Compare to NNLO y_H distributions, we observe large reduction of scale variation band for more than 50% at N^{3}LO. The scale variation band at N^{3}LO stays within the NNLO band with a flat k factor about 1.035 in the central rapidity region ($|y_H| \leq 3.6$). Both the systematic error analysis and the phenomenology predictions confirm that our calculations at

N^{3}LO using q_T subtraction formalism are well under control. The approximation related to the C_{N3} coefficient in our approach can be easily replaced by the full analytical results which would be available in the near future.

With the exception of larger data set and more accurate measurements of Higgs properties at LHC, we prepare precise theoretical tools that could match the frontier accuracy of experiment results. More differential properties at N^{3}LO involving the Higgs boson and its decay products can be studied using the same framework established in this paper. The current N^{3}LO calculation under heavy top assumption is resolving the precision that finite top mass effects need to be considered. We would leave the discussion for those effects to future studies.

Acknowledgements

LC would like to thank Stefano Catani for very useful and valuable discussions. XC would like to thank Javier Mazzitelli and Hua Xing Zhu for inspiring discussion. We thank the University of Zurich S3IT and CSCS Lugano for providing the computational resources for this project. This research was supported in part by the UK Science and Technology Facilities Council, by the Swiss National Science Foundation (SNF) under contracts 200020-175595 and CRSII2-160814, by the Swiss National Supercomputing Centre (CSCS) under project ID UZH10, by the Research Executive Agency (REA) of the European Union under the ERC Advanced Grant MC@NNLO (340983).

Appendix

A Convolutions at N^{3}LO

The numerical implementation of Eq. (7) requires the computation of several convolutions between splitting functions, collinear and helicity-flip functions. In principle, taking the N-moments of the functions involved in the calculation, one can avoid the use of convolutions, since in N-space they are simply products. However the numerical implementation of Eq. (7) on the Monte Carlo code `HN3LO` was carried out in the z-space (e.g as in the codes `HNNLO` [1], `DYNNLO` [42], `2`γ`NNLO` [43], etc), and therefore the new third order convolutions have to be calculated as well.

The convolutions in Eqs. (34), (35), (41) and (44) between two functions ($f(z)$ and $g(z)$) of the the variable z are defined through the following integral

$$(f \otimes g)(z) \equiv \int_z^1 \frac{dy}{y}\, f\left(\frac{z}{y}\right)\, g(y)\,. \tag{46}$$

In the case of processes initiated by gluon fusion, the complete list of third order convolutions to be calculated can be found in Table 3. All the remaining convolutions in Eq. (7) at N^{3}LO already contributed to the previous orders and they are regarded as known. The symbol $\gamma_{ab}^{(n)}$ in Table 3 denotes the usual splitting functions of n-order and they contribute to Eq. (7) since the PDFs have to be evolved from the scale b_0^2/b^2 to the customary factorization scale μ_F. The first three rows in Eq. (3) were calculated in Ref. [45] and cross checked with a dedicated computation for the results presented in this paper. The `Mathematica` public code `MT` [44] used to calculate

(i)	$\gamma^{(1)}_{ga_1} \otimes \gamma^{(1)}_{a_1 a_2} \otimes \gamma^{(1)}_{a_2 g}$	(ii)	$\gamma^{(1)}_{ga_1} \otimes \gamma^{(1)}_{a_1 a_2} \otimes \gamma^{(1)}_{a_2 q}$
(iii)	$\gamma^{(1)}_{ga} \otimes \gamma^{(2)}_{ag}$	(iv)	$\gamma^{(1)}_{ga} \otimes \gamma^{(2)}_{aq}$
(v)	$\gamma^{(2)}_{ga} \otimes \gamma^{(1)}_{ag}$	(vi)	$\gamma^{(2)}_{ga} \otimes \gamma^{(1)}_{aq}$
(vii)	$C^{(1)}_{ga} \otimes \gamma^{(2)}_{ag}$	(viii)	$C^{(1)}_{ga} \otimes \gamma^{(2)}_{aq}$
(ix)	$C^{(2)}_{ga} \otimes \gamma^{(1)}_{ag}$	(x)	$C^{(2)}_{ga} \otimes \gamma^{(1)}_{aq}$
(xi)	$G^{(1)}_{ga} \otimes \gamma^{(1)}_{ag}$	(xii)	$G^{(1)}_{ga} \otimes \gamma^{(1)}_{aq}$

Table 3: *Convolutions appearing at the N^3LO exclusively between the collinear $C^{(n)}_{a_1a_2}$, the helicity-flip $G^{(n)}_{a_1a_2}$ and the splitting functions $\gamma^{(n)}_{a_1a_2}$ ($n = 1, 2$). The repeated subindices a, a_1 and a_2 imply a sum over the parton flavors $q, \bar{q}, g$. The first and last subindices denote the partonic channel in which they are contributing, i.e the convolutions in the first column are used in the gg partonic channel whereas the second (and last) column is for the qg and gq partonic channels.*

the necessary convolutions (i)–(vi) in Ref. [45] is allowed to provide the resulting convolutions in terms of *Harmonic Poly–Logarithms* (HPLs) [47] exploiting the `Mathematica` package `HPL` [46]. The remaining convolutions in Eqs. (vii)–(xii) of Table 3 were computed in particular for this work. The `MT` [44] package is not able to solve all the convolutions of weight 3 and 4 that are needed in (vii)–(xii). For instance the `MT` package can not handle convolutions in which their result has to be expressed in terms of multiple poly–logarithms (or *Goncharov Poly–Logarithms* GPLs) [48, 49] as it is the case when the collinear functions $C^{(2)}_{gj}$ are involved. Owing to the precedent reasons we computed the convolutions (vii)–(xii) with the code `Convo` which is able to provide results in terms of GPLs and also can handle with terms separately divergent but finite after addition.

The multiple poly–logarithms can be defined recursively, for $n \geq 0$, via the iterated integral [48, 49]

$$G(a_1, \ldots, a_n; z) = \int_0^z \frac{dt}{t - a_1} G(a_2, \ldots, a_n; t) , \tag{47}$$

with $G(z) = G(; z) = 1$ (an exception being when $z = 0$ in which case we put $G(0) = 0$) and with $a_i \in \mathbb{C}$ are chosen constants and z is a complex variable. Nevertheless, for the convolutions in Table 3 the following conditions verify: the variable $z \in \mathbb{R}$ and the weights $a_1, \ldots, a_n \in \mathbb{R}$.

Among the required convolutions in Table 3 we list some of them which appear as building blocks in the course of the computation of Eqs. (vii)–(xii) in Table 3,

$$\left\{ \mathrm{D}_0[1-y]; \frac{1}{y}; 1; y; y^2 \right\} \otimes \left(\frac{f(y)}{1+y} \right) \quad , \tag{48}$$

$$\begin{aligned} f(y) = \Bigg\{ &\mathrm{Li}_3\left(\frac{1}{1+y}\right); \mathrm{Li}_3(\pm y); \mathrm{Li}_2(\pm y); \mathrm{Li}_2(1-y); \mathrm{Li}_2(\pm y)\ln(y); \\ &\ln^2(1+y)\ln(y); \ln(1+y)\ln^2(y) \Bigg\} \quad , \end{aligned} \tag{49}$$

(a)	$G(\frac{z}{1+z},0,0,1;\frac{1}{2})$	(b)	$G(1,0,0,-z;z)$	(c)	$G(0,1,0,-1;z)$
(d)	$G(0,1,0,z;1)$	(e)	$G(0,1,z,0;1)$	(f)	$G(0,z,1,0;1)$
(g)	$G(-z,0,z,0;1)$	(h)	$G(0,1,0,-z;z)$	(i)	$G(0,1,-z,-z;z)$
(j)	$G(-z,1,0,0;1)$	(k)	$G(-z,1,0,0;z)$	(l)	$G(-z,0,0,z;1)$

Table 4: *Basis for the GPLs used in the numerical implementation of the convolutions listed in Table 3. The basis is not unique, however its length is enough for a straightforward numerical implementation in the Monte Carlo generator.*

where the customary *plus* distribution $\mathrm{D}_0[1-z]$ is defined as usual

$$\int_0^1 dz\ f(z)\ \mathrm{D}_0[1-z] = \int_0^1 dz\ \frac{f(z)}{(1-z)_+} = \int_0^1 \frac{dz}{1-z}\left(f(z)-f(1)\right)\ . \tag{50}$$

After performing all the convolutions listed in Table 3, their final expressions (each one of the convolutions) are finite in the domain $z \in (0,1)$. Even more, convolutions when evaluated in the domain $z \in (0,1)$ produce results belonging to $\mathbb{R}$. It is possible to write the expressions in Table 3 (after simplifying) in function of twelve GPLs that are not reducible to *classic* functions or can not be combined (e.g through the *shuffle* algebra) with other GPLs in order to produce simpler results. Here the adjective *classic* is used to mean functions that do not require the numerical implementation of specific packages to handle GPLs or HPLs, for instance: $\mathrm{Li}_i(z)$ $(0 \le i \le 4)$ and polynomials of the variable $(0 \le z \le 1)$.

The list of the irreducible GPLs is presented in Table 4. All the other GPLs appearing in the resulting convolutions of Table 3 can be related to the set of Table 4 using the results of Refs. [51, 46, 50] and performing the customary *shuffle* algebra. The numerical implementation of the GPLs in Table 4 was made using the package `GiNaC` [52]. The basis of GPLs in Table 4 is not unique, but its present form is enough for a reasonable numerical evaluation *event-by-event*.

As an example of a third order convolution we can perform the following integral

$$\begin{aligned}
&\left(\frac{\mathrm{Li}_3(y)}{1+y}\otimes \mathrm{D}_0[1-y]\right)(z) = \int_z^1 \frac{dy}{y+z}\,\mathrm{Li}_3\left(\frac{z}{y}\right)\,\frac{1}{(1-y)_+} = \frac{1}{1+z}\bigg(-\zeta_3 G(0;z) + \frac{i\pi^3}{6}G(0;z)\\
&+\frac{\pi^2}{3}G(-z;1)G(0;z) - i\pi G(-z,0;1)G(0;z) - G(-z,0,0;1)G(0;z) + \frac{i\pi\zeta_3}{4} + \frac{\pi^2}{3}G(0,1;z)\\
&+i\pi G(-z;1)G(0,0;z) - \frac{\pi^2}{6}G(0,0;z) - G(-z;1)G(0,0,0;z) + i\pi G(0,0,1;z)\\
&+G(0,0;z)G(-z,0;1) - \frac{\pi^2}{3}G(-z,0;1) + i\pi G(-z,0,0;1) - G(0,0,0,1;z)\\
&-G(0,0,1,z;1) - G(0,0,z,1;1) - G(0,1,0,z;1) - G(1,0,0,z;z) + G(-z,0,0,0;1)\\
&-G(-z,0,0,z;1) + G(-z,0,0,z;z) + \frac{19\pi^4}{720}\bigg)\ .
\end{aligned} \tag{51}$$

Notice that with the rescaling property of the GPLs

$$G(k\,(a_1\ldots a_n);k\,x) = G(a_1\ldots a_n;x) \qquad \text{with}\ \ (a_n \neq 0)\ \ \text{and}\ \ (k\in\mathbb{C}^*)\ , \tag{52}$$

it is possible to write some GPLs in Eq. (51) as HPLs. After performing all the convolutions in Table 3 and applying the precedent properties (satisfied by the GPLs), it is possible to arrive to the set detailed in Table 4. The rescaling property of Eq. (52) can be used also to relate the GPL in Eq. (l) in Table 4 with the one in Eq. (c) of the same Table (*modulo* functions of the type $\mathrm{Li}_i(z)$ $(0 \leq i \leq 4)$ and polynomials in the variable $(0 \leq z \leq 1)$) after some algebra. However this procedure leads to the numerical evaluation of Eq. (c) in Table 4 in a different argument $(1/z)$, which from a purely numerical point of view, does not represent any improvement. Therefore the GPL basis in Table 4 has to be taken as irreducible in a numerical sense, since it represents the smallest numerical cost *event-by-event*.

References

[1] S. Catani and M. Grazzini, Phys. Rev. Lett. **98** (2007) 222002 [hep-ph/0703012].

[2] G. Bozzi, S. Catani, D. de Florian and M. Grazzini, Nucl. Phys. B **737** (2006) 73 [hep-ph/0508068].

[3] G. Bozzi, S. Catani, D. de Florian and M. Grazzini, Phys. Lett. B **564** (2003) 65.

[4] R. Boughezal, C. Focke, X. Liu and F. Petriello, Phys. Rev. Lett. **115** (2015) 062002 [arXiv:1504.02131 [hep-ph]].

[5] J. Gaunt, M. Stahlhofen, F. J. Tackmann and J. R. Walsh, JHEP **1509** (2015) 058 [arXiv:1505.04794 [hep-ph]].

[6] F. Dulat, B. Mistlberger and A. Pelloni, JHEP **1801** (2018) 145 doi:10.1007/JHEP01(2018)145 [arXiv:1710.03016 [hep-ph]].

[7] A. Gehrmann-De Ridder, T. Gehrmann and E. W. N. Glover, JHEP **0509** (2005) 056 [hep-ph/0505111]; A. Gehrmann-De Ridder, T. Gehrmann and E. W. N. Glover, Phys. Lett. B **612** (2005) 49 [hep-ph/0502110]; A. Gehrmann-De Ridder, T. Gehrmann and E. W. N. Glover, Phys. Lett. B **612** (2005) 36 [hep-ph/0501291]; A. Daleo, T. Gehrmann and D. Maitre, JHEP **0704** (2007) 016 [hep-ph/0612257]; A. Daleo, A. Gehrmann-De Ridder, T. Gehrmann and G. Luisoni, JHEP **1001** (2010) 118 [arXiv:0912.0374 [hep-ph]]; R. Boughezal, A. Gehrmann-De Ridder and M. Ritzmann, JHEP **1102** (2011) 098 [arXiv:1011.6631 [hep-ph]]; T. Gehrmann and P. F. Monni, JHEP **1112** (2011) 049 [arXiv:1107.4037 [hep-ph]]; A. Gehrmann-De Ridder, T. Gehrmann and M. Ritzmann, JHEP **1210** (2012) 047 [arXiv:1207.5779 [hep-ph]]; J. Currie, E. W. N. Glover and S. Wells, JHEP **1304** (2013) 066 [arXiv:1301.4693 [hep-ph]].

[8] Y. L. Dokshitzer, D. Diakonov and S. I. Troian, Phys. Lett. B **79** (1978) 269, Phys. Rep. **58** (1980) 269; G. Parisi and R. Petronzio, Nucl. Phys. B **154** (1979) 427. G. Curci, M. Greco and Y. Srivastava, Nucl. Phys. B **159** (1979) 451; J. C. Collins and D. E. Soper, Nucl. Phys. B **193** (1981) 381 [Erratum-ibid. B **213** (1983) 545], Nucl. Phys. B **197** (1982) 446; J. Kodaira and L. Trentadue, Phys. Lett. B **112** (1982) 66, report SLAC-PUB-2934 (1982), Phys. Lett. B **123** (1983) 335; J. C. Collins, D. E. Soper and G. Sterman, Nucl. Phys. B **250** (1985) 199; S. Catani, E. D'Emilio and L. Trentadue, Phys. Lett. B **211** (1988) 335; D. de Florian and M. Grazzini, Phys. Rev. Lett. **85** (2000) 4678 [arXiv:hep-ph/0008152];

S. Catani, D. de Florian and M. Grazzini, Nucl. Phys. B **596** (2001) 299 [arXiv:hep-ph/0008184].

[9] W. Bizon, P. F. Monni, E. Re, L. Rottoli and P. Torrielli, JHEP **1802** (2018) 108 doi:10.1007/JHEP02(2018)108 [arXiv:1705.09127 [hep-ph]].

[10] S. Catani and M. Grazzini, Nucl. Phys. B **845** (2011) 297 [arXiv:1011.3918 [hep-ph]].

[11] S. Catani, L. Cieri, D. de Florian, G. Ferrera and M. Grazzini, Nucl. Phys. B **881** (2014) 414 doi:10.1016/j.nuclphysb.2014.02.011 [arXiv:1311.1654 [hep-ph]].

[12] S. Catani, D. de Florian and M. Grazzini, Nucl. Phys. B **596** (2001) 299 [arXiv:hep-ph/0008184].

[13] O. V. Tarasov, A. A. Vladimirov and A. Y. Zharkov, Phys. Lett. **93B** (1980) 429. doi:10.1016/0370-2693(80)90358-5

[14] S. A. Larin and J. A. M. Vermaseren, Phys. Lett. B **303** (1993) 334 doi:10.1016/0370-2693(93)91441-O [hep-ph/9302208].

[15] D. de Florian and M. Grazzini, Nucl. Phys. B **616** (2001) 247 [arXiv:hep-ph/0108273].

[16] S. Catani and M. Grazzini, Eur. Phys. J. C **72** (2012) 2013 [Erratum-ibid. C **72** (2012) 2132] [arXiv:1106.4652 [hep-ph]].

[17] S. Catani, L. Cieri, D. de Florian, G. Ferrera and M. Grazzini, Eur. Phys. J. C **72** (2012) 2195 [arXiv:1209.0158 [hep-ph]].

[18] G. Curci, W. Furmanski and R. Petronzio, Nucl. Phys. B **175** (1980) 27.

[19] W. Furmanski and R. Petronzio, Phys. Lett. B **97** (1980) 437.

[20] R. V. Harlander and K. J. Ozeren, Phys. Lett. B **679** (2009) 467 [arXiv:0907.2997 [hep-ph]];

[21] S. Catani, E. D'Emilio and L. Trentadue, Phys. Lett. B **211** (1988) 335. doi:10.1016/0370-2693(88)90912-4

[22] R. P. Kauffman, Phys. Rev. D **45** (1992) 1512. doi:10.1103/PhysRevD.45.1512

[23] D. de Florian and M. Grazzini, Phys. Rev. Lett. **85** (2000) 4678 doi:10.1103/PhysRevLett.85.4678 [hep-ph/0008152].

[24] D. de Florian and M. Grazzini, Nucl. Phys. B **616** (2001) 247 doi:10.1016/S0550-3213(01)00460-6 [hep-ph/0108273].

[25] X. Chen *et al.*, arXiv:1805.00736 [hep-ph].

[26] W. Bizo *et al.*, arXiv:1805.05916 [hep-ph].

[27] M. Spira, A. Djouadi, D. Graudenz and P. M. Zerwas, Nucl. Phys. B **453** (1995) 17 [hep-ph/9504378].

[28] Y. Li and H. X. Zhu, Phys. Rev. Lett. **118** (2017) no.2, 022004 doi:10.1103/PhysRevLett.118.022004 [arXiv:1604.01404 [hep-ph]].

[29] A. A. Vladimirov, Phys. Rev. Lett. **118** (2017) no.6, 062001 doi:10.1103/PhysRevLett.118.062001 [arXiv:1610.05791 [hep-ph]].

[30] S. Catani, L. Cieri, D. de Florian, G. Ferrera and M. Grazzini, Nucl. Phys. B **888** (2014) 75 doi:10.1016/j.nuclphysb.2014.09.012 [arXiv:1405.4827 [hep-ph]].

[31] T. Becher, M. Neubert, Eur. Phys. J. **C71** (2011) 1665 [arXiv:1007.4005 [hep-ph]].

[32] F. Wilczek, Phys. Rev. Lett. **39** (1977) 1304;
M. A. Shifman, A. I. Vainshtein and V. I. Zakharov, Phys. Lett. B **78** (1978) 443;
T. Inami, T. Kubota and Y. Okada, Z. Phys. C **18** (1983) 69.

[33] R. D. Ball *et al.* [NNPDF Collaboration], JHEP **1504** (2015) 040 [arXiv:1410.8849].

[34] A. Buckley, J. Ferrando, S. Lloyd, K. Nordstrm, B. Page, M. Rfenacht, M. Schnherr and G. Watt, Eur. Phys. J. C **75** (2015) 132 doi:10.1140/epjc/s10052-015-3318-8 [arXiv:1412.7420 [hep-ph]].

[35] X. Chen, T. Gehrmann, E. W. N. Glover and M. Jaquier, Phys. Lett. B **740** (2015) 147 doi:10.1016/j.physletb.2014.11.021 [arXiv:1408.5325 [hep-ph]].

[36] X. Chen, J. Cruz-Martinez, T. Gehrmann, E. W. N. Glover and M. Jaquier, JHEP **1610** (2016) 066 doi:10.1007/JHEP10(2016)066 [arXiv:1607.08817 [hep-ph]].

[37] A. Gehrmann-De Ridder, T. Gehrmann, E. W. N. Glover, A. Huss and T. A. Morgan, Phys. Rev. Lett. **117** (2016) no.2, 022001 doi:10.1103/PhysRevLett.117.022001 [arXiv:1507.02850 [hep-ph]].

[38] A. Gehrmann-De Ridder, T. Gehrmann, E. W. N. Glover, A. Huss and T. A. Morgan, JHEP **1611** (2016) 094 doi:10.1007/JHEP11(2016)094 [arXiv:1610.01843 [hep-ph]].

[39] A. Gehrmann-De Ridder, T. Gehrmann, E. W. N. Glover, A. Huss and D. M. Walker, Phys. Rev. Lett. **120** (2018) no.12, 122001 doi:10.1103/PhysRevLett.120.122001 [arXiv:1712.07543 [hep-ph]].

[40] B. Mistlberger, arXiv:1802.00833 [hep-ph].

[41] F. Dulat, A. Lazopoulos and B. Mistlberger, arXiv:1802.00827 [hep-ph].

[42] S. Catani, L. Cieri, G. Ferrera, D. de Florian and M. Grazzini, Phys. Rev. Lett. **103** (2009) 082001 doi:10.1103/PhysRevLett.103.082001 [arXiv:0903.2120 [hep-ph]].

[43] S. Catani, L. Cieri, D. de Florian, G. Ferrera and M. Grazzini, Phys. Rev. Lett. **108** (2012) 072001 Erratum: [Phys. Rev. Lett. **117** (2016) no.8, 089901] doi:10.1103/PhysRevLett.108.072001, 10.1103/PhysRevLett.117.089901 [arXiv:1110.2375 [hep-ph]].

[44] M. Hschele, J. Hoff, A. Pak, M. Steinhauser and T. Ueda, Comput. Phys. Commun. **185** (2014) 528 doi:10.1016/j.cpc.2013.10.007 [arXiv:1307.6925 [hep-ph]].

[45] M. Hschele, J. Hoff, A. Pak, M. Steinhauser and T. Ueda, Phys. Lett. B **721** (2013) 244 doi:10.1016/j.physletb.2013.03.003 [arXiv:1211.6559 [hep-ph]].

[46] D. Maitre, Comput. Phys. Commun. **174** (2006) 222 doi:10.1016/j.cpc.2005.10.008 [hep-ph/0507152].

[47] E. Remiddi and J. A. M. Vermaseren, Int. J. Mod. Phys. A **15** (2000) 725 doi:10.1142/S0217751X00000367 [hep-ph/9905237].

[48] A. B. Goncharov, Math. Res. Lett. **5** (1998) 497 doi:10.4310/MRL.1998.v5.n4.a7 [arXiv:1105.2076 [math.AG]].

[49] A. B. Goncharov, math/0103059 [math.AG].

[50] C. Duhr, H. Gangl and J. R. Rhodes, JHEP **1210** (2012) 075 doi:10.1007/JHEP10(2012)075 [arXiv:1110.0458 [math-ph]].

[51] H. Frellesvig, D. Tommasini and C. Wever, JHEP **1603** (2016) 189 doi:10.1007/JHEP03(2016)189 [arXiv:1601.02649 [hep-ph]].

[52] C. W. Bauer, A. Frink and R. Kreckel, J. Symb. Comput. **33** (2000) 1 [cs/0004015 [cs-sc]].